USGS
science for a changing world

Prepared in cooperation with the
U.S. Department of Energy,
under Interagency Agreements
DE-AI08-92NV10874 and DE-AI08-97NV12033

Analysis of Conservative Tracer Tests in the Bullfrog, Tram, and Prow Pass Tuffs, 1996 to 1998, Yucca Mountain, Nye County, Nevada

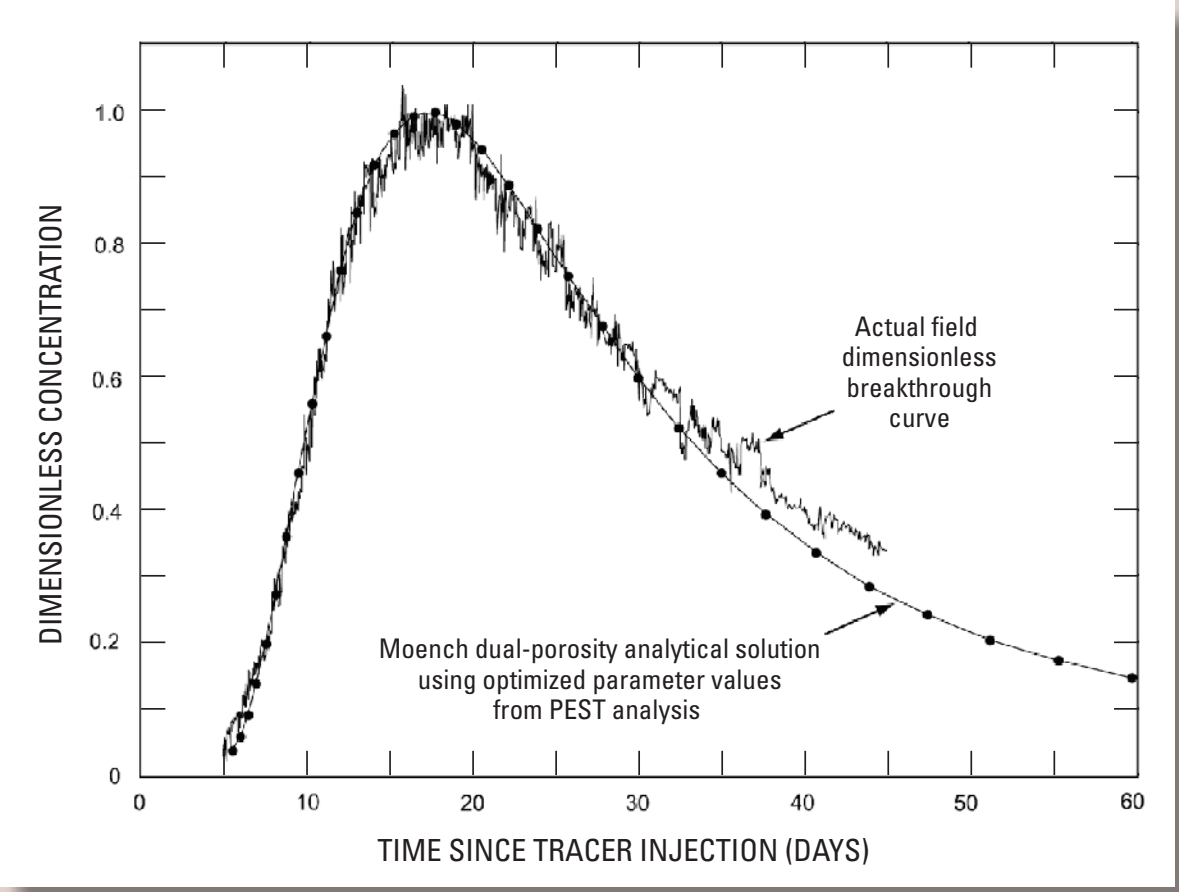

Scientific Investigations Report 2007–5280

U.S. Department of the Interior
U.S. Geological Survey

Analysis of Conservative Tracer Tests in the Bullfrog, Tram, and Prow Pass Tuffs, 1996 to 1998, Yucca Mountain, Nye County, Nevada

By Amjad Umari, Michael F. Fahy, John D. Earle, and Patrick Tucci

Prepared in cooperation with the
U.S. Department of Energy,
under Interagency Agreements
DE-AI08-92NV10874 and DE-AI08-97NV12033

Scientific Investigations Report 2007–5280

U.S. Department of the Interior
U.S. Geological Survey

U.S. Department of the Interior
DIRK KEMPTHORNE, Secretary

U.S. Geological Survey
Mark D. Myers, Director

U.S. Geological Survey, Reston, Virginia: 2008

About USGS Products

For product and ordering information:
World Wide Web: http://www.usgs.gov/pubprod
Telephone: 1-888-ASK-USGS

For more information on the USGS—the Federal source for science about the Earth, its natural and living resources, natural hazards, and the environment:
World Wide Web: http://www.usgs.gov
Telephone: 1-888-ASK-USGS

About this Product

For more information concerning this publication, contact:
Chief, USGS, Yucca Mountain Project Branch
Box 25046
Denver Federal Center
MS 421
Denver, CO 80225-0046
(303) 236-5050

This publication is available online at:
http://pubs.er.usgs.gov/usgspubs/index

Publishing support provided by:
Denver Publishing Service Center, Denver, Colorado
Manuscript approved for publication, September 2007
Edited by Mary A. Kidd and Pamela B. Daddow
Layout by Sharon Powers

Suggested citation:

Umari, Amjad, Fahy, Michael F., Earle, John D., and Tucci, Patrick, 2008, Analysis of conservative tracer tests in the Bullfrog, Tram, and Prow Pass Tuffs, 1996 to 1998, Yucca Mountain, Nye County, Nevada: U.S. Geological Survey Scientific Investigations Report 2007–5280, 40 p.

Any use of trade, product, or firm names is for descriptive purposes only and does not imply endorsement by the U.S. Government.

Although this report is in the public domain, permission must be secured from the individual copyright owners to reproduce any copyrighted materials contained within this report.

Contents

Figures

Tables

Conversion Factors and Datum

Multiply	By	To obtain
centimeter (cm)	0.3937	inch
gram (g)	2.205×10^{-3}	pound
kilogram (kg)	2.205	pound
kilometer (km)	0.62139	mile
liter (L)	0.26417	gallon
liter per minute (L/min)	0.26417	gallon per minute
liter per second (L/s)	15.85	gallon per minute
meter (m)	3.2808	foot
microgram per liter (μg/L)	1	part per billion
micrometer (μm)	3.937×10^{-5}	inch
milligram (mg)	2.205×10^{-6}	pound
milligram per liter (mg/L)	1	part per million
nanogram per liter (ng/L)	1	part per trillion
square meter	10.76	square foot

The following abbreviations are for basic dimensions:

Length: [*L*]
Time: [*T*]
Mass: [*M*]

Concentration given variably as mg/L, μg/L, or ng/L as appropriate for the range of concentration being discussed or graphically displayed.

Temperature in degrees Celsius (°C) may be converted to degrees Fahrenheit (°F) as follows:

$$°F=(1.8\times°C)+32$$

Sea level: Altitudes in this report are referenced to the National Geodetic Vertical Datum of 1929 (NGVD of 1929), a geodetic datum derived from a general adjustment of the first-order level nets of the United States and Canada, formerly called “the Sea Level Datum of 1929” or “mean sea level.”

Analysis of Conservative Tracer Tests in the Bullfrog, Tram, and Prow Pass Tuffs, 1996 to 1998, Yucca Mountain, Nye County, Nevada

By Amjad Umari, Michael F. Fahy, John D. Earle, and Patrick Tucci

Abstract

To evaluate the potential for transport of radionuclides in ground water from the proposed high-level nuclear-waste repository at Yucca Mountain, Nevada, conservative (nonsorbing) tracer tests were conducted among three boreholes, known as the C-hole Complex, and values for transport (or flow) porosity, storage (or matrix) porosity, longitudinal dispersivity, and the extent of matrix diffusion were obtained. The C-holes are completed in a sequence of Miocene tuffaceous rock, consisting of nonwelded to densely welded ash-flow tuff with intervals of ash-fall tuff and volcaniclastic rocks, covered by Quaternary alluvium. The lower part of the tuffaceous-rock sequence includes the Prow Pass, Bullfrog, and Tram Tuffs of the Crater Flat Group. The rocks are pervaded by tectonic and cooling fractures. Paleozoic limestone and dolomite underlie the tuffaceous rocks.

Four radially convergent and one partially recirculating conservative (nonsorbing) tracer tests were conducted at the C-hole Complex from 1996 to 1998 to establish values for flow porosity, storage porosity, longitudinal dispersivity, and extent of matrix diffusion in the Bullfrog and Tram Tuffs and the Prow Pass Tuff. Tracer tests included (1) injection of iodide into the combined Bullfrog-Tram interval; (2) injection of 2,6 difluorobenzoic acid into the Lower Bullfrog interval; (3) injection of 3-carbamoyl-2-pyridone into the Lower Bullfrog interval; and (4) injection of iodide and 2,4,5 trifluorobenzoic acid, followed by 2,3,4,5 tetrafluorobenzoic acid, into the Prow Pass Tuff. All tracer tests were analyzed by the Moench single- and dual-porosity analytical solutions to the advection-dispersion equation or by superposition of these solutions. Nonlinear regression techniques were used to corroborate tracer solution results, to obtain optimal parameter values from the solutions, and to quantify parameter uncertainty resulting from analyzing two of the three radially convergent conservative tracer tests conducted in the Bullfrog and Tram intervals.

Longitudinal dispersivity values in the Bullfrog and Tram Tuffs ranged from 1.83 to 2.6 meters, flow-porosity values from 0.072 to 0.099, and matrix-porosity values from 0.088 to 0.19. The flow-porosity values indicate that the pathways between boreholes UE-25 c#2 and UE-25 c#3 in the Bullfrog and Tram intervals are not connected well.

Tracer testing in the Prow Pass interval indicates different transport characteristics than those obtained in the Bullfrog and Tram intervals. In the Prow Pass Tuff, longitudinal dispersivity was 0.27 meter, flow porosity was 4.5×10^{-4}, and matrix porosity was 0.01. This indicates that the flow network in the Prow Pass is dominated by interconnected fractures, whereas in the Bullfrog and Tram, the flow network is dominated by discontinuous fractures with connecting segments of matrix.

Introduction

Yucca Mountain, located about 145 kilometers (km) northwest of Las Vegas in southern Nevada (fig. 1), is the site designated by the U.S. Department of Energy (DOE) to store high-level nuclear waste in a proposed mined, underground repository. To evaluate the potential for transport of radionuclides in ground water from the proposed repository area, conservative (nonsorbing) tracer tests were conducted among three boreholes known as the C-hole Complex (fig. 1), and estimates of transport porosity (or flow porosity), storage porosity (or matrix porosity), longitudinal dispersivity, and the extent of matrix diffusion (the dimensionless diffusion coefficient) were obtained. The C-hole Complex has been extensively described in Geldon (1993, 1996) and Geldon and others (1998, 2002). A range of transport parameters was sought by conducting tracer tests in the high-transmissivity Bullfrog Tuff and Tram Tuff and in the low-transmissivity Prow Pass Tuff, all of Miocene age. The results of these tracer tests are presented as part of a series of investigations by the U.S. Geological Survey (USGS) regarding the hydrologic and geologic characteristics of Yucca Mountain. This investigation was conducted in cooperation with the U.S. Department of Energy (DOE), under Interagency Agreements DE-AI08-92NV10874 and DE-AI08-97NV12033.

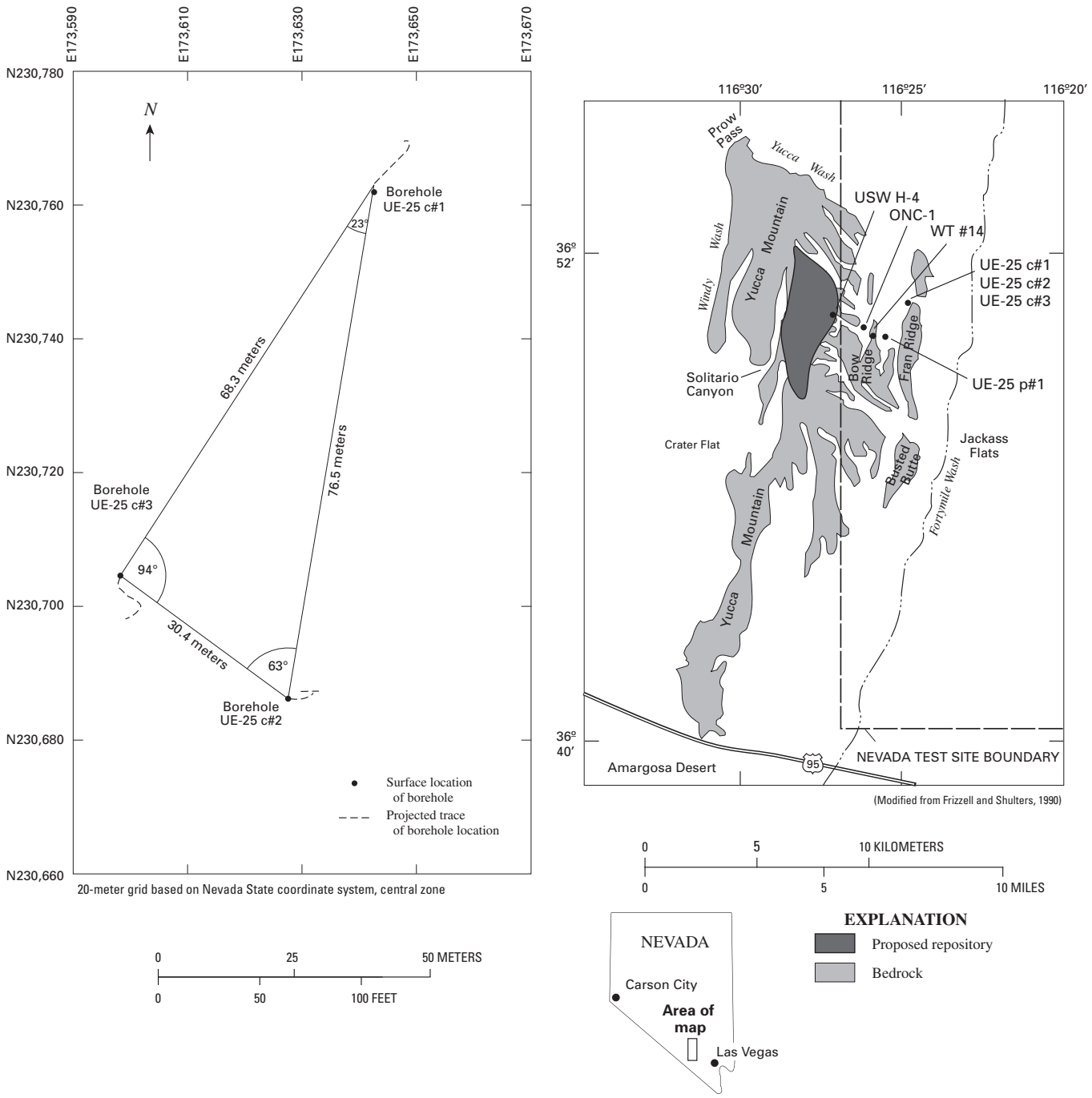

Figure 1. Location of the C-hole Complex, boreholes UE-25 c#1, UE-25 c#2, and UE-25 c#3, and nearby boreholes.

Purpose and Scope

This report presents the results of four convergent tracer tests and one partially recirculating tracer test in Miocene tuffaceous rocks in three boreholes at the C-hole Complex at Yucca Mountain, Nevada. The tests were conducted with conservative tracers from February 1996 to September 1998 to determine the transport porosity (or flow porosity), matrix porosity (or storage porosity), and longitudinal dispersivity of the Bullfrog, Tram, and Prow Pass Tuffs. The report describes the tests that were conducted, breakthrough curves (BTCs) for injected tracers, and analyses performed on the test data; presents values of transport properties determined from test analyses; summarizes conceptual models of solute transport in the Bullfrog and Tram Tuffs compared to the Prow Pass Tuff; and evaluates uncertainties and limitations associated with the test data, analyses, and quantitative results.

Previous Work

Hydrogeologic intervals at the C-hole Complex were identified initially by Geldon (1996) on the basis of borehole geophysical logs, borehole flow surveys, cross-hole seismic tomography, and aquifer tests that were conducted in 1983–84. Hydraulic tests and associated flow surveys conducted in 1995–97 are documented in Geldon and others (1998, 2002).

Hydraulic properties of the hydrogeologic intervals in the C-holes, such as matrix porosity, matrix permeability, hydraulic conductivity, transmissivity, and storativity, were determined by Geldon (1993, 1996) from geophysical logs, laboratory analyses, and aquifer tests. The barometric efficiency and effective porosity of the C-holes were established (Geldon and others, 1997). An open-hole hydraulic test, conducted in borehole UE-25 c#3 from May 22 to June 12, 1995 (Geldon and others, 1998), was designed to determine the transmissivity, hydraulic conductivity, and storativity of the composite saturated thickness of Miocene tuffaceous rocks at the C-hole Complex, lateral variations in hydraulic properties within a 2-mile radius of the C-hole Complex, and possible hydraulic connection between the Miocene tuffaceous rocks and an underlying regional aquifer composed of Paleozoic carbonate rocks (Geldon and others, 2002).

A series of hydraulic tests was conducted at the C-hole Complex from June 1995 through November 1997, prior to and in conjunction with the tracer tests discussed in this report. Water levels in several wells near the C-hole Complex were monitored during the hydraulic tests and were used in the analyses of the tests. Geldon and others (2002) describe those tests and analyses, present the hydraulic properties (transmissivity and storativity) obtained, and describe changes in water chemistry during the tests.

Acknowledgments

The authors wish to thank Drs. Jake Turin and Amr Abdel-Fattah of Los Alamos National Laboratory for their excellent technical reviews. This report reflects the improvement from their input.

Hydrogeologic Setting at the C-hole Complex

The C-hole Complex was constructed in 1983–84 in the channel of an ephemeral stream that cuts through Bow Ridge, a spur of Yucca Mountain (fig. 2). The C-holes are 30.4 to 76.5 meters (m) apart at land surface (fig. 1); however, because of borehole deviation during drilling, interborehole distances at depth range from 28.6 to 86.3 m (Geldon and others, 1997, p. 2). The C-holes are completed in Miocene tuffaceous rocks (table 1 and fig. 3) that are covered by 0 to 24 m of Quaternary alluvium. The tuffaceous rocks are estimated to be 1,040 to 1,590 m thick in the vicinity of the C-holes, where they consist of nonwelded to densely welded ash-flow tuff with intervals of ash-fall tuff and volcaniclastic rocks (Geldon, 1993; Geldon and others, 1998). The lower part of the tuffaceous rock sequence includes the Prow Pass, Bullfrog, and Tram Tuffs of the Crater Flat Group. The tuffaceous rocks are pervaded by tectonic and cooling fractures that strike predominantly north-northeast to north-northwest and dip westward at angles of 50 to 87 degrees (Geldon, 1996, p. 4). Paleozoic limestone and dolomite (Carr and others, 1986) penetrated by borehole UE-25 p#1, which is about 600 m southeast of the C-hole Complex (fig. 2), underlie the tuffaceous rocks and are estimated to be about 455 m below the bottom of the C-holes. For more detail on the hydrogeologic setting of the C-holes, see Geldon and others (2002, p. 4).

Tracer Tests at the C-hole Complex

Four tracer tests were conducted by the USGS at the C-hole Complex using tracers that are conservative with respect to the tuffaceous rocks at the complex: (1) injection of iodide into the combined Lower Bullfrog–Upper Tram interval (called the Bullfrog-Tram interval); (2) injection of 2,6 difluorobenzoic acid (2,6 DFBA) into the Lower Bullfrog interval; (3) injection of 3-carbamoyl-2-pyridone (pyridone) into the Lower Bullfrog interval; and (4) injection of iodide and 2,4,5 trifluorobenzoic acid (2,4,5 TFBA), followed by 2,3,4,5 tetrafluorobenzoic acid (2,3,4,5 TeFBA), in the Prow Pass Tuff. Los Alamos National Laboratory also conducted tracer tests at the C-hole Complex using tracers that are both conservative and nonconservative (“reactive” or sorbing) with respect to the tuffaceous rocks at the complex (Bechtel-SAIC Company, 2003). These tests are not discussed in this report.

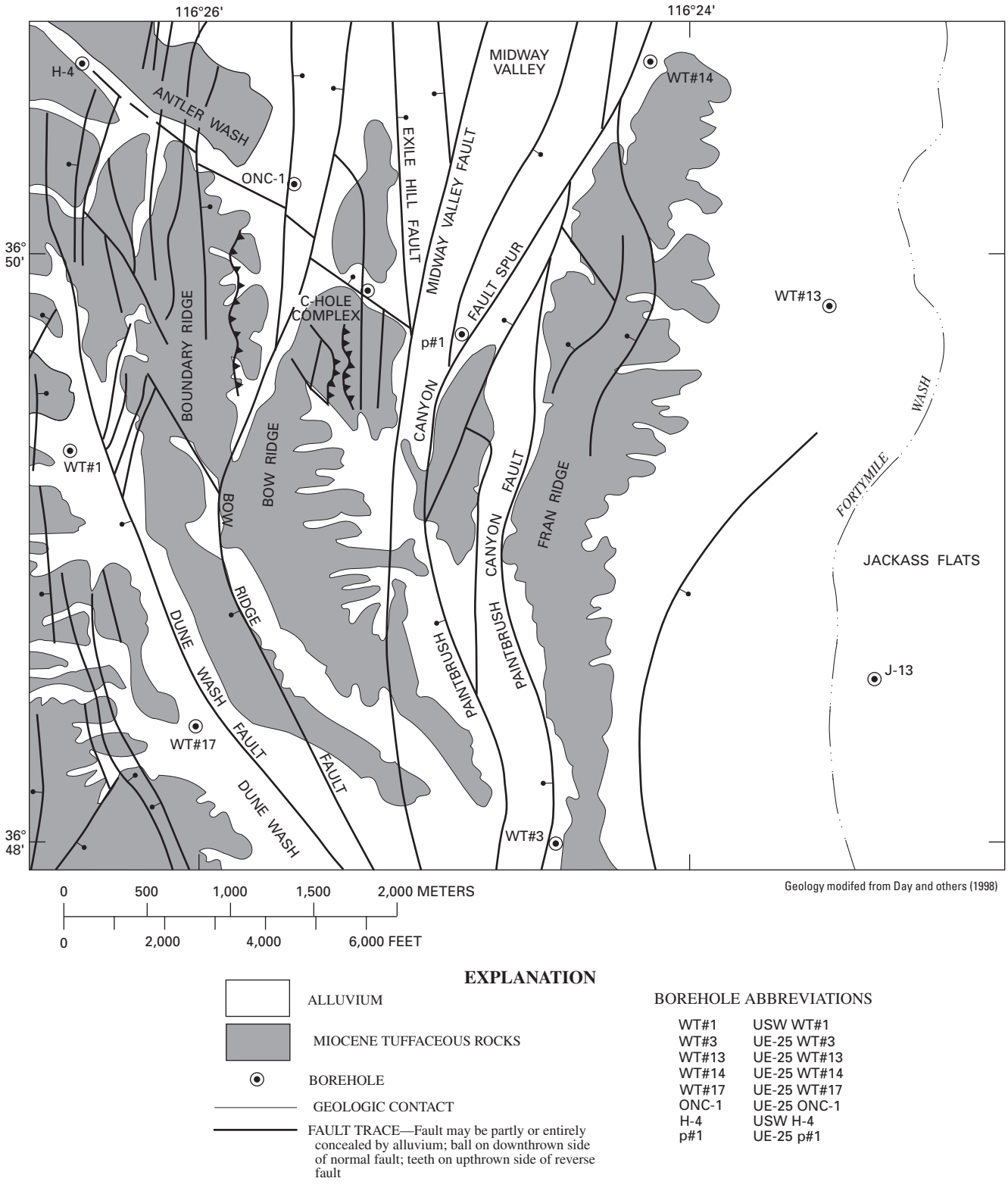

Figure 2. Generalized geologic map showing the location of the C-hole Complex and nearby boreholes.

Table 1. Stratigraphy of Miocene tuffaceous rocks in the C-hole area.
[Modified from table 1, p. 6, Geldon and others, 1998]

Geologic unit	Depth below land surface, in meters		
	UE-25 c#1	UE-25 c#2	UE-25 c#3
Paintbrush Group			
Tiva Canyon Tuff	0–96	21–88	24–88
Topopah Spring Tuff	96–406	88–401	88–396
Calico Hills Formation	406–516	401–510	396–496
Crater Flat Group			
Prow Pass Tuff	516–656	510–652	496–644
Bullfrog Tuff	656–828	652–829	644–814
Tram Tuff	828–914+	829–914+	814–914+

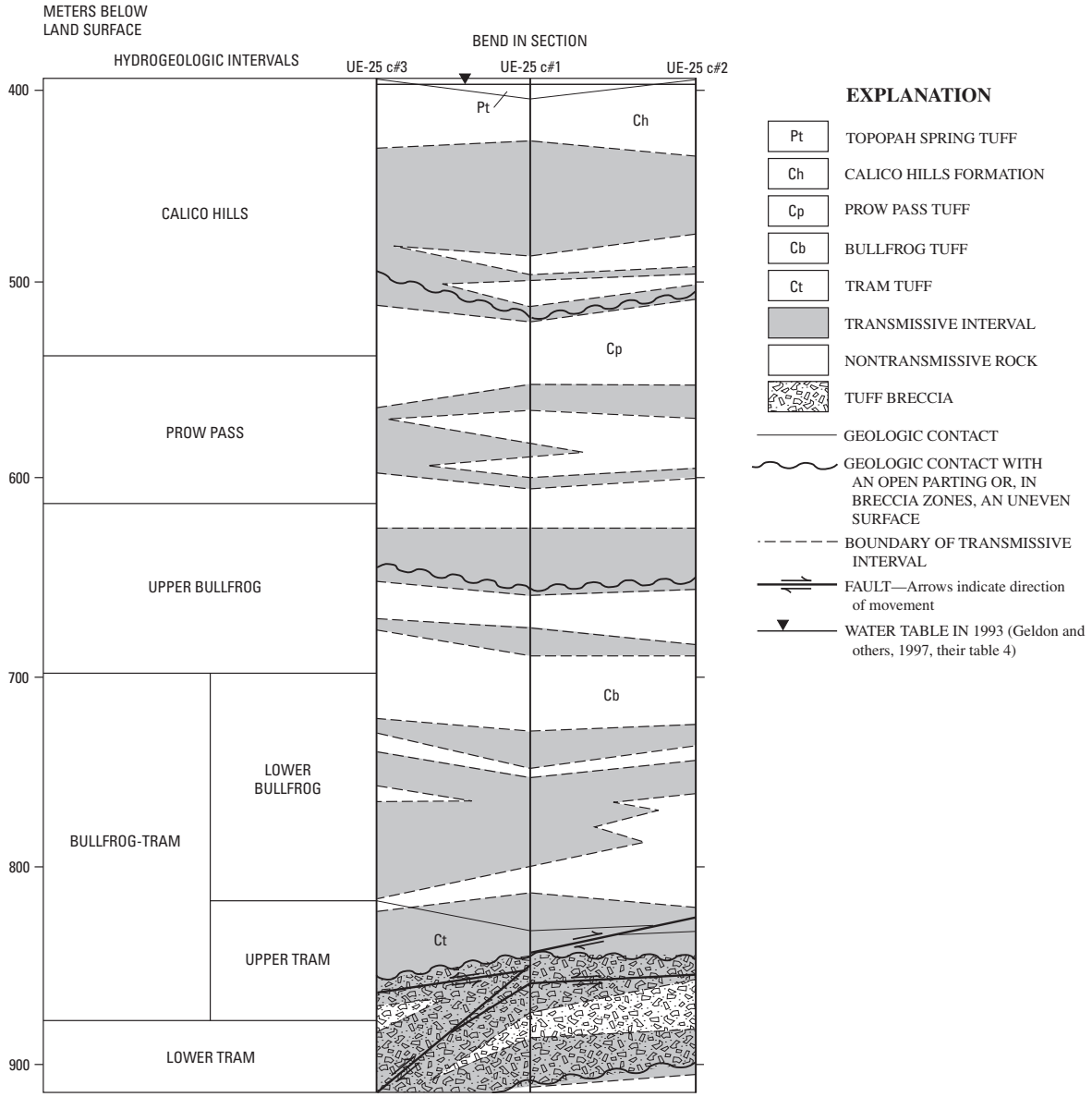

Figure 3. Hydrogeologic intervals in the C-holes.

Field and Laboratory Methods

The purpose of the field testing was to establish flow porosity, storage porosity, and longitudinal dispersivity of the Bullfrog-Tram interval, the Lower Bullfrog Tuff, and the Prow Pass Tuff by using conservative tracers. The approach to developing the parameters was to conduct multiple cross-hole tests and to use multiple analytical solution methods to interpret the results. The results were in the form of BTCs (concentrations plotted against time) of the various tracers. In these cross-hole tracer tests, a known mass of tracer is injected into the interval being tested at one well, the injection well, while another well, the production well, is pumped at some rate. In the Prow Pass tracer tests, the test interval fluid was mixed by pumping it to the surface, where it could be sampled, and then back to the test interval. If some, or all, of the water pumped from the production well is reinjected into the injection well, the test is called a partially or fully recirculating tracer test; otherwise it is called a radially convergent tracer test. For either case, prior to tracer injection, pumping from the production well and, if applicable, reinjection of the pumped water into the injection well, is conducted until a quasi-steady-state flow field is established as determined from pressure sensors in the wells (this was done whether it is explicitly stated in the description of each test or not). The tracer travels from the injection to the production well where it is gradually pumped from the tested interval. At the surface, some of the pumped water is diverted to an automated sampler that collects specified amounts of water (samples) at specified time intervals. The automated sampler is controlled by a personal-computer (PC)-based program described in Geldon and others (2002, p. 14).

The concentrations of iodide, benzoic acids (2,6 DFBA; 2,4,5 TFBA; and 2,3,4,5 TeFBA), and pyridone in a water sample can be obtained by reverse-phase high-pressure liquid chromatography (HPLC) in conjunction with an ultraviolet (UV)-absorption detector (Stetzenbach and Thompson, 1983). This method was selected not only because it is precise and sensitive, but also because the instruments are portable and the ground-water samples can be injected directly into the instrument. These features allow preliminary analyses to be conducted in the field for immediate test results. Tracer concentrations were confirmed later in the laboratory. Field-determined tracer detection limits, and field-determined accuracy and precision of the HPLC analytical technique were obtained only for the tracer tests in the Bullfrog-Tram and Lower Bullfrog intervals. The field-determined detection limit was 3 micrograms per liter (μg/L) for iodide; 40 μg/L for 2,6 DFBA; and 0.1 μg/L for pyridone.

The accuracy of the HPLC analytical technique was calculated as the difference between the nominal and measured concentrations of standards divided by the nominal concentration. These calculated accuracy values were as follows: iodide, ±3.47 percent for field analyses and ±2.67 percent for laboratory analyses; 2,6 DFBA, 2,4,5 TFBA, and 2,3,4,5 TeFBA, ±10 percent for laboratory analyses; and pyridone, ±7 percent for laboratory analyses. HPLC runs of tracer "standards" prepared at specific concentrations, used to create the calibration curves to convert from HPLC raw readings to tracer concentrations, are done against a blank fluid stream moving through the HPLC system, whereas the runs of standards used for this accuracy calculation are interspersed among runs of different water samples.

The precision of the HPLC analytical technique, as determined by comparing replicate analyses, was as follows: iodide, ±2.30 percent for field-determined concentrations and ±1.61 percent for laboratory-determined concentrations; 2,6 DFBA, 2,4,5 TFBA, and 2,3,4,5 TeFBA, ±10 percent for laboratory-determined concentrations; and pyridone, ±10 percent for laboratory-determined concentrations greater than 100 nanograms per liter (ng/L) and exceeding ±10 percent for laboratory-determined concentrations less than 100 ng/L.

Analytical Solution Methods

All tracer tests were analyzed with the Moench single-porosity (Moench, 1989) or dual-porosity (Moench, 1995) analytical solution to the advection-dispersion equation for radially convergent, areal flow for a single- or dual-porosity, homogeneous, isotropic medium, or by superposition of these solutions. Multiple solutions were used to ensure that the appropriate solution method was used in matching a particular set of data and to determine whether the aquifer behaves as a single- or dual-porosity aquifer. The fractured tuff at the C-hole Complex has been conceptualized for this report as an equivalent porous medium (EPM) that is either a single-porosity medium or dual-porosity medium. A single-porosity medium is conceptualized as consisting of only a flowing-water component, made up of interconnected fractures and discontinuous fractures that have connecting segments of matrix (fig. 4). The porosity of the flowing-water component is referred to as the "flow porosity." A dual-porosity medium is conceptualized as consisting of both a flowing-water component and an immobile-water component. The immobile-water component (or storage component) is made up of dead-end fractures and the part of the matrix not contributing to the flow network. The porosity of the immobile-water component is referred to as the "storage porosity" or "matrix porosity." The flowing-water component of an EPM is represented by a longitudinal dispersivity and a flow porosity, and the immobile-water component is represented by a storage porosity and a dimensionless matrix-diffusion coefficient. A PC-based graphical user interface was developed by the USGS to perform pre- and postprocessing for the Moench analytical solutions (Umari, 1996). The input parameters required by the Moench single-porosity or dual-porosity solution are:

- production rate, q_o [L^3/T]
- distance from the production well to the injection well, r_L [L]
- aquifer thickness, h [L]

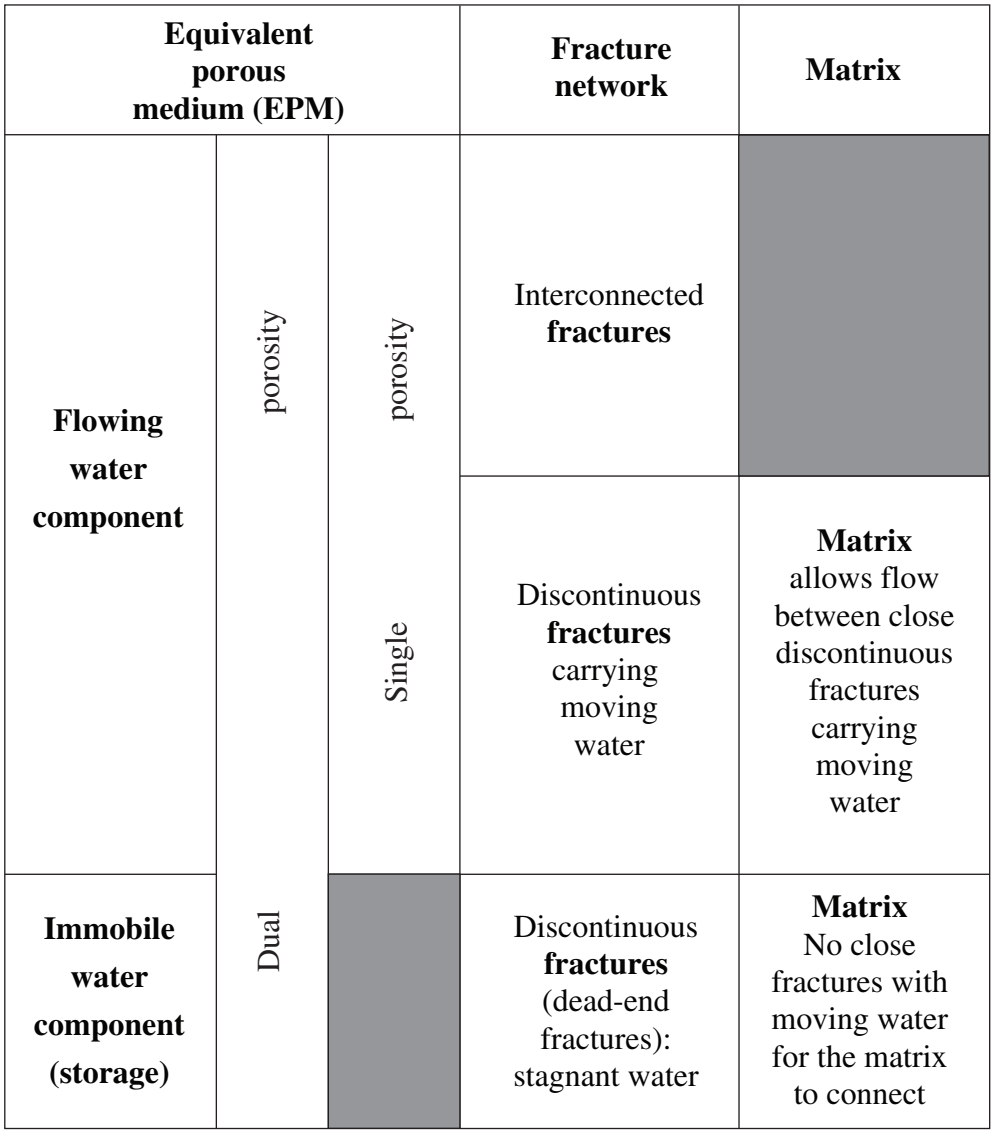

Figure 4. Conceptual diagram of the flowing and immobile water components of an equivalent porous medium (EPM) in a fractured rock mass.

- radius of the production well, r_w [L]; and the injection well, r_i [L]
- mixing length in the production well, h_w [L]; and the injection well, h_i [L]. The length within the borehole through which the tracer is assumed to enter or exit the surrounding aquifer. For this report, the mixing length is assumed to be equal to the length of the transmissive intervals (based on previously conducted geophysical logs and (or) hydraulic tests) within the packed-off interval during a tracer test
- mass of tracer injected, M' [M]
- volume of water in which the tracer is dissolved prior to entering the aquifer, V' [L^3]
- length of time for the tracer slug to enter the aquifer, t_{inj} [T], which is assumed to be equal to the duration of tracer injection into the borehole of the injection well. It is used for calculating a Moench type curve for analyzing radially convergent tracer tests except when the tracer injection is assumed to be instantaneous as

is explained later for analyzing the recirculating tracer tests in this report

- flow porosity, ϕ_f, and matrix porosity, ϕ' [dimensionless]. Matrix porosity is referred to interchangeably as "storage porosity" in this report
- longitudinal dispersivity, α_L [L], in the form of the dimensionless Peclet number, $PE = r_L/\alpha_L$. Longitudinal dispersivity is a measure of the ability of a porous medium to disperse a solute along streamlines (groundwater flow lines)
- retardation coefficient representing linear, reversible adsorption, R, in the fractures; R', in the matrix [dimensionless]. Because all the tracers used were conservative (nonsorbing), a retardation coefficient of 1.0 was used for all solutions
- dimensionless diffusion coefficient, GAMMA (γ), diffusion of a solute into the matrix (immobile-water component of the EPM). GAMMA (γ) is a function of the effective coefficient of diffusion from the fractures into the matrix, D', and of h, ϕ_f, R, q_o, and the radius, b', of the theoretical sphere-shaped matrix blocks of the dual-porosity medium. It also is a function of r_L and r_w (Moench, 1995, table 1, p. 1826)
- dimensionless storage coefficient, SIGMA (σ), which is a function of ϕ_f, ϕ', R, and R'
- dimensionless skin parameter, SK, which is a function of D', b', and the mass transfer coefficient (k_s), the latter representing the continuity of diffusive flux across the "skin" (such as mineral coatings on fracture surfaces separating fractures from matrix blocks)

In a radially convergent flow field, the volume of interest is a cylinder centered at the pumping borehole and extending to the injection borehole. The volume of water in the pores of this cylinder is $\pi h\phi_f(r_L^2 - r_w^2)$. The time that it would take to pump this amount of water at the rate of q_o is referred to as the advection traveltime, t_a, and is given by the equation (Moench, 1989, table 1, p. 441):

$$t_a = \pi h\phi_f(r_L^2 - r_w^2) / q_o \qquad (1)$$

The advection traveltime, t_a, represents the length of time for a tracer slug to travel from the injection well to the production well by plug flow (pure advection: no dispersion, $\alpha_L = 0$).

To approximate the effects of mixing in the injection well, Moench (1989) used the hypothesis that the average value of the tracer concentration over this large cylindrical surface area equals the tracer concentration of the well-mixed fluid in the injection borehole multiplied by a constant (epsilon, ε, eq. 8, p. 441). Epsilon represents the fraction of the water withdrawn by the production well that passes through the injection well.

To perform the Moench analysis, curves of theoretical tracer concentrations versus time at the production well are compared to curves of actual field tracer concentrations as a function of time at the production well. Specifically, type curves for the Moench analytical solution methods for radially convergent flow were generated for a range of Peclet numbers. These single-porosity and dual-porosity type curves are in the form of log-log plots of theoretical dimensionless concentration, C_D, versus theoretical dimensionless time, $t_D = t/t_a$, where t is the dimensional time since injection. $C_D = C/C_i$ for the case of a finite-duration pulse considered in this report, where C [M/L^3] is the dimensional concentration, and C_i [M/L^3] is a reference concentration defined as (Moench, 1989, table 1, p. 441):

$$C_i = M' / [\pi h\phi_f(r_L^2 - r_w^2)] \qquad (2)$$

The actual field tracer breakthrough concentrations plotted as a function of elapsed dimensional time since injection (or actual field dimensional BTCs) are converted to log-log plots of normalized concentration, c/c_{max} (where the concentration is normalized by the maximum observed concentration) versus dimensional time since injection, hereinafter referred to as actual field dimensionless BTCs. By overlaying the type curve and actual field dimensionless BTC and matching the rising portions of the two curves, estimates of t_a (and through equation 1, ϕ_f) and PE (Peclet number) are obtained. The estimate of t_a is obtained when the match point ($t_D = 1$, $C_D = 1$) is projected onto the log-time axis of the actual field dimensionless BTC (shown in fig. 5 for the tracer test described in the following section). Because dimensionless time is defined as the ratio of time since injection to t_a, the value of t_a is equal to the time since injection, indicated on the time axis of the actual field dimensionless BTC, corresponding to t_D=1. The PE value generating the type curve that best matches the rising limb is considered the estimated PE. If the medium is conceptualized as a single-porosity medium and the Moench single-porosity type curve was used to match the rising limb, the matching is complete (Matching Method 1). This method of obtaining t_a and PE from matching the rising limb with a type curve also can be performed by matching the rising limb of the single-porosity theoretical BTC to the rising limb of the actual BTC. t_a is varied to move the theoretical BTC horizontally along the dimensional time axis, and PE is varied to change the shape of the rising limb until a good match with the rising limb of the actual BTC is obtained. Even for a medium that is well represented by the Moench single-porosity analytical solution, Matching Method 1 may result in a close match of the rising limb but not of the falling limb. The falling limb match may not be very good but may be good enough to assert that the medium is a single-porosity medium.

If the falling limb match is not very good, it may be possible to improve the match by using Matching Method 2. In this method, t_a and PE are varied until a loose match is obtained of the whole BTC. To obtain a better overall match of the rising and falling limbs to the whole actual BTC, t_a and

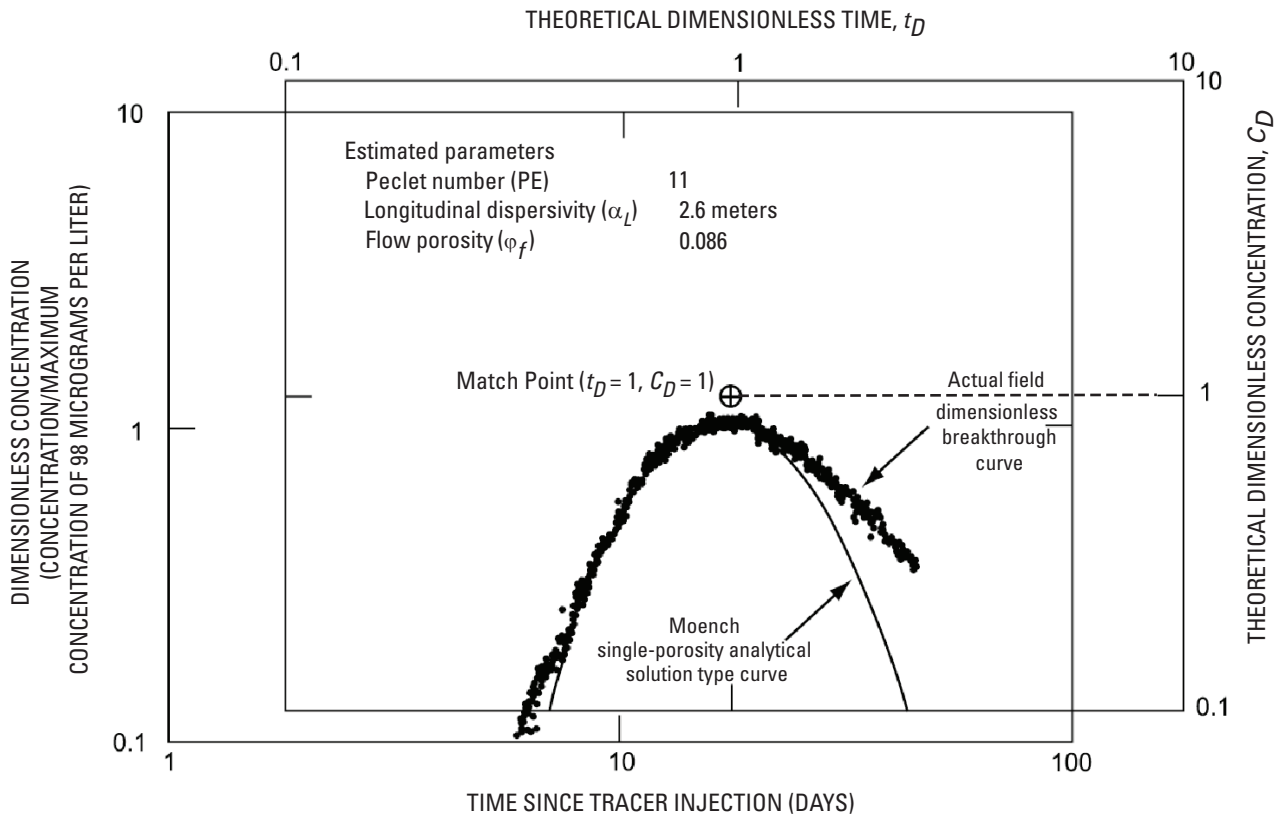

Figure 5. Visual match of the actual field breakthrough curve to the Moench (1989) single-porosity analytical solution type curve for the iodide tracer test in the Bullfrog-Tram interval (Matching Method 1).

PE can be varied such that the single-porosity type curve or theoretical BTC loosely matches the whole actual BTC (for the type-curve match, type curves of different PE values are overlain loosely until one with a corresponding match point and associated t_a is chosen). This will be referred to as Matching Method 2.

If Matching Method 2 cannot match the falling limb of the actual BTC, then the aquifer may be a dual-porosity medium and the Moench dual-porosity solution should be used. For a dual-porosity medium, PE also is estimated first by matching the rising-limb part of the type curve for either the single- or dual-porosity solution. The PE value generating the type curve that best matches the rising-limb part of the actual field dimensionless BTC is considered the "estimated" PE. In this process of estimating the PE from the rising-limb type-curve match, the assumption is made that in a dual-porosity aquifer, and therefore in the dual-porosity solution, diffusion is minimal on the rising limb of the BTC and, therefore, PE is the main influence on the shape of the rising limb (Moench, 1995, p. 1831) and the single- and dual-porosity solutions are essentially the same.

This process of estimating t_a and PE also can be performed by matching the rising limbs of either the single- or dual-porosity theoretical BTC to the rising limb of the actual BTC, such as in figure 6 for the analysis of the tracer test described in the following section. t_a is varied to move the theoretical BTC horizontally along the dimensional time axis, and PE is varied to change the shape of the rising limb until a good match with the actual BTC is obtained. The falling limb of the actual BTC in figure 5 can be matched to a theoretical dual-porosity BTC with diffusion processes in which the controlling parameters include the dimensionless diffusion coefficient, GAMMA, and the SIGMA term, which is a function of the matrix porosity, ϕ' (fig. 6). To match the falling limb, the optimal values of t_a and PE obtained from matching the rising limb are used, then GAMMA and SIGMA are varied and their values estimated from a match of the falling limb. This visual graphical matching process is referred to as Matching Method 3.

In cases where the assumption that "in a dual-porosity aquifer, diffusion is minimal on the rising limb of a BTC" is not valid for the tracer test being analyzed, Matching Method 3 may result in a close match for only the rising limb, and the tail may diverge substantially. In these cases, t_a and (or) PE may be varied from their rising-limb match values, along with SIGMA and GAMMA, when matching the falling limb (Matching Method 4). This may result in a "loose" match, but it generally leads to improved overall matches of the whole BTC, and estimates of all four parameters (t_a, PE, SIGMA, GAMMA) are obtained. This match, referred to as a global

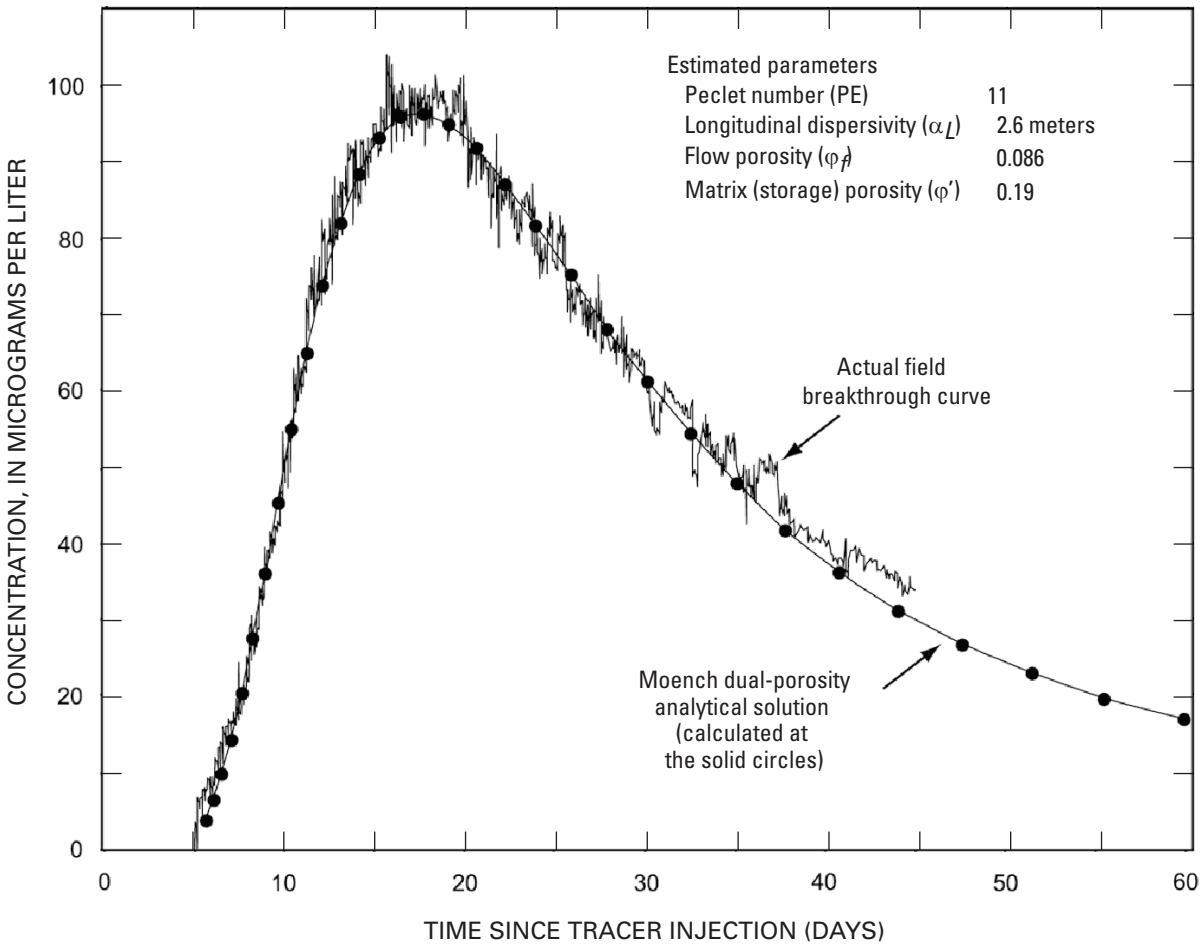

Figure 6. Visual match of the actual field breakthrough curve to the Moench (1995) dual-porosity analytical solution for the iodide tracer test in the Bullfrog-Tram interval (Matching Method 3).

match because it does not favor matching the rising limb or the falling limb, can be performed visually by graphical matching or mathematically by the nonlinear regression technique, PEST, explained below.

In summary, four methods were used to obtain matches. In Matching Method 1 for a single-porosity medium, t_a and PE are first obtained from a close match of the rising limb by using the Moench single-porosity analytical solution. The falling limb match may not be very good, but good enough to assert that the medium is a single-porosity medium. If the falling limb match is not very good, it may be possible to improve it by using Matching Method 2. In this method, t_a and PE are varied until a loose match is obtained of the whole BTC.

If Matching Method 2 cannot match the falling limb, then the Moench dual-porosity solution can be used as Matching Method 3 where t_a and PE, again, are first obtained from a close match of the rising limb. With these values of t_a and PE fixed, the parameters SIGMA and GAMMA are then varied and their values estimated from a match of the falling limb. In this method, parts of the match, notably the rising limb, are very close and others, notably the tail, may diverge significantly. Only visual graphical matching (as opposed to PEST matching) is used in Matching Method 3.

In Matching Method 4, t_a and PE are first obtained from a close match of the rising limb with the Moench dual-porosity solution, as in Matching Method 3. With these values of t_a and PE used as starting values, SIGMA and GAMMA, along with t_a and (or) PE, are varied and estimates of all four parameters are obtained from matching the whole BTC (both rising and falling limbs). Even though in this method some parts of the match may be loose compared to Matching Method 3, the overall match for the whole BTC is generally better. Both visual graphical matching and (or) PEST matching (explained below) are used in Matching Method 4.

Some of the analyses of conservative tracer tests in this report used the single-porosity Moench solution, some used the dual-porosity Moench solution, and some used a combination of both, depending on the type of test. The purpose of this multiple-analysis approach was to ensure that the appropriate solution method is used in matching a particular set of data

and to determine whether the aquifer behaves as a single- or dual-porosity aquifer.

In addition to graphical matching techniques, nonlinear regression techniques were used in this report to match theoretical BTCs to actual BTCs. Nonlinear regression techniques have been used for many years to determine optimal transport parameters (for example, Umari, 1977; Umari and others, 1979; Wagner and Gorelick, 1986; Medina and Carrera, 1996; and Anderman and Hill, 1999). In this report, nonlinear regression techniques, in the form of a parameter-estimation software program (PEST; Watermark Computing, 1994), were used to supplement the analyses conducted with graphical matching techniques using the Moench single- and dual-porosity solutions. PEST was used to corroborate tracer-test solution results, to obtain optimal parameter values from the solutions, and to quantify parameter uncertainty resulting from analyzing two of the three radially convergent conservative tracer tests in the Bullfrog and Tram Tuffs. The third test had only a rising limb of the BTC and was not suitable for optimization by PEST. PEST was implemented so that it executes the Moench analytical solution. Initial estimates of PE, SIGMA, and GAMMA were provided to PEST from a visual match, and PEST was instructed to keep one of the three parameters constant while varying the other two. PEST repeatedly executed the Moench solution until it obtained optimal parameters that minimized the sum of the squares of the differences between actual and theoretical concentrations. PEST was always run with the ϕ_f obtained from the visual graphical match. The above process is referred to as PEST matching.

Tracer Tests in the Bullfrog and Tram Tuffs

Tracer tests conducted in the Bullfrog and Tram Tuffs at the C-holes consisted of: (1) injection of iodide into the combined Lower Bullfrog–Upper Tram interval, (2) injection of 2,6 DFBA into the Lower Bullfrog interval, and (3) injection of pyridone into the Lower Bullfrog interval. The iodide test was conducted while the production well, UE-25 c#3, was pumped continuously from February 8, 1996, to March 31, 1996. The other two tests were conducted starting in January 1997, and well UE-25 c#3 was pumped continuously from May 8, 1996, to November 12, 1997.

Iodide Tracer Test in the Lower Bullfrog–Upper Tram Interval

The most transmissive interval in the C-holes (the Bullfrog-Tram interval), the shortest interborehole distance (from borehole UE-25 c#2 to borehole UE-25 c#3), and the simplest flow field (a radially convergent flow field) were selected for the first tracer test at the C-holes to enhance the possibility of successful tracer recovery (see fig. 1). Following establishment of a quasi-steady-state hydraulic gradient by pumping the production well (UE-25 c#3) for about 7,000 minutes (4.86 days), the first tracer test at the C-hole Complex was initiated in the Bullfrog-Tram interval on February 13, 1996, under convergent flow field conditions (also discussed in Fahy, 1997). Tracer solution was injected into the packed-off Bullfrog-Tram interval (about 170 m thick, fig. 3) of borehole UE-25 c#2 for 28 minutes at an average rate of 0.41 liter per second (L/s).

The tracer solution consisted of 5.9 kilograms (kg) of sodium iodide (of which 5.0 kg was iodide) dissolved in 500 L of water from borehole UE-25 c#3. Chemical analysis indicated that the tracer solution had an iodide concentration of 10,200 milligrams per liter (mg/L). The tracer solution was chased with 182 L of water from UE-25 c#3, which was pumped into borehole UE-25 c#2 to enhance the evacuation of the tracer slug out of the borehole and into the aquifer. The tracer was detected in samples from borehole UE-25 c#3 5.07 days after injection, and the average peak concentration of approximately 98 µg/L occurred 17.8 days after injection. The test was terminated on March 29, 1996, 45.1 days after injection. The mass recovered was estimated as 2.35 kg, about 47 percent of the injected mass.

The tracer test was complicated by progressively decreasing discharge from the recovery well, which was caused by a mechanically failing pump. The pump discharge decreased from 8.5 L/s on February 13, 1996, to 6.2 L/s on March 29, 1996 (Bechtel-SAIC Company, 2003, section 6.3.5.1). For analysis, the average value of 7.4 L/s was used as the discharge rate. Despite this problem, a recovery curve, with breakthrough and peak arrival times readily discernible, was established clearly by March 29, 1996 (figs. 5, 6, 7).

Both the single- and dual-porosity Moench solutions (Moench, 1989, 1995) were used to interpret this test. The rising limb was first analyzed using the single-porosity solution and Matching Method 1 to obtain t_a (and, through equation 1, ϕ_f) and the Peclet number (fig. 5). The falling limb did not match well, so the dual-porosity solution and Matching Method 3 then were used with these estimated parameter values to match the falling limb (fig. 6) to obtain GAMMA and SIGMA, the latter a function of the matrix porosity. Input parameters and results are:

- discharge rate of 7.4 L/s
- aquifer thickness 51.2 m, equal to the transmissive thickness of the Bullfrog-Tram interval between boreholes UE-25 c#2 and UE-25 c#3 (Geldon and others, 2002, table 8, p. 35)
- Peclet number of 11, which corresponds to a longitudinal dispersivity (α_L) of about 2.6 m (figs. 5 and 6)
- advection traveltime, t_a, of 18.5 days

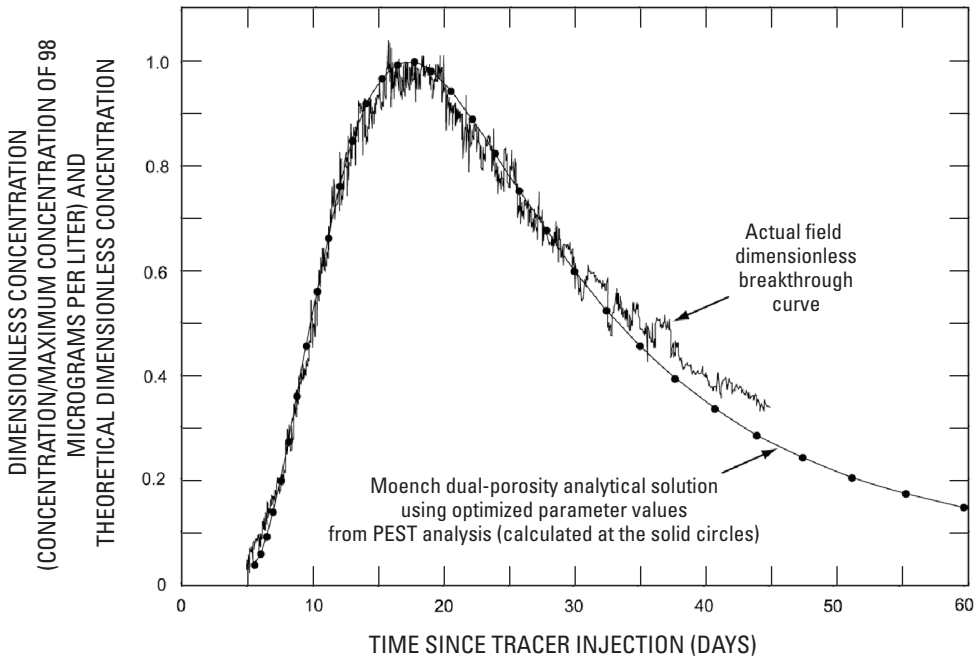

EXPLANATION

Initial parameter estimates from the visual match of these data (fig. 6)

PEST-optimized parameter results (with 95-percent confidence intervals)

Peclet number (PE)	11.478 (11.228–11.728)
Dimensionless storage coefficient (SIGMA)	1.717 (1.435–2.000)
Dimensionless diffusion coefficient (GAMMA)	0.03565 (0–0.1274)
Other estimated parameters	
Longitudinal dispersivity (α_L)	2.52 meters
Flow porosity (φ_f)	0.086
Matrix (storage) porosity (φ')	0.16

Figure 7. PEST-optimized match of the actual field breakthrough curve to the Moench (1995) dual-porosity analytical solution for the iodide tracer test in the Bullfrog-Tram interval (Matching Method 4).

- flow porosity, ϕ_f, estimated as 0.086. This flow porosity estimate is high if fractures are considered as the only pathway. Typical fracture porosities range from 10^{-2} to 10^{-5} (see, for example, Freeze and Cherry, 1979, p. 408). The high flow-porosity value indicates that a composite pathway occurs for the iodide; that is, the fracture network is not connected well at the scale of the test. The solute travels through a connected-fracture-network segment, then through a segment of matrix until it reaches the next connected-fracture-network segment

- using Matching Method 3 and matching the falling limb (fig. 6) results in an estimate of GAMMA = 0.04, and SIGMA = 2.0, the latter resulting in an estimate of 0.19 for the matrix (storage) porosity (ϕ') This estimated matrix porosity is reasonable based on geophysical logging conducted at the C-hole Complex that resulted in a range of total porosity (sum of matrix and flow porosity) from 0.12 to 0.43 (Geldon, 1993, p. 60–62)

In addition to the best visual graphical matches of figures 5 and 6 presented above, the parameter-estimation program PEST (Watermark Computing, 1994) was used to obtain a match by minimizing the sum of squares of the differences between actual and theoretical concentrations. The PEST analysis, consisting of several runs, started with the values resulting from the visual graphical match presented in figure 6, which are: PE = 11, SIGMA = 2.0, and GAMMA = 0.04. Each run varied one of these parameters while the others were held constant. In the first run, PEST was given the values

PE = 11, SIGMA = 1.0 (changed from its best-visual-match value of 2.0), and GAMMA = 0.04, and only SIGMA could be changed. PEST values for PE, SIGMA, and GAMMA are more accurate than visual match values and are, therefore, given to 5 significant figures for PE and 4 for SIGMA and GAMMA, as opposed to 2 for visual match values. PEST converged on an optimal value of SIGMA = 1.717. In the second run, PEST was given the values PE = 8 (changed from its best-visual-match value of 11), SIGMA = 1.717, and GAMMA = 0.04, and only PE could be changed. PEST converged on an optimal value of PE = 11.478. In the third run, PEST was given the values PE = 11.478, SIGMA = 1.717, and GAMMA = 1.0 (changed from its best-visual-match value of 0.04), and only GAMMA could be changed. PEST converged on an optimal value of GAMMA = 0.03565. The PEST match of the Moench dual-porosity solution using the above optimal values to the actual BTC and the associated confidence intervals of the optimal values are shown in figure 7.

The estimated parameters resulting from the visual graphical match of figure 6 and the PEST match of figure 7 are quite close. The Peclet number and dispersivity estimates vary by approximately 4 percent. The visual-graphical-match matrix porosity estimate is 0.19, and the PEST match estimate is 0.16. The difference in values is attributed to the different emphasis given to fitting portions of the BTC. Matching method 3 was used for the visual graphical match of figure 6, where the rising limb is used exclusively to estimate the Peclet number and the advection traveltime, and then the advection traveltime is used to estimate the flow porosity. Matching Method 4 was used for the PEST match of figure 7, where the match is optimized to both rising- and falling-limb data. This results in slightly different matches. The transport properties obtained from the conservative tracer testing in the Bullfrog-Tram interval for the iodide test from borehole UE-25 c#2 to UE-25 c#3 with radially convergent flow are summarized in table 2.

2,6 Difluorobenzoic Acid Tracer Test in the Lower Bullfrog Interval

On January 10, 1997, a radially convergent conservative tracer test was initiated between the same boreholes as the iodide tracer test, UE-25 c#2 to UE-25 c#3, but only in the 97-m-thick Lower Bullfrog interval. Approximately 11.4 kg of 2,6 DFBA, dissolved in 795 L of water from borehole UE-25 c#3, was injected for 28 minutes at an average rate of 0.52 L/s into the Lower Bullfrog interval in borehole UE-25 c#2, followed by 238 L of rinsate (from rinsing the tracer-solution tank) and chase water from a tank of water previously pumped from UE-25 c#3. Chemical analysis indicated that the 2,6 DFBA injectate solution had a concentration of 15,560 mg/L.

Breakthrough of the tracer occurred at borehole UE-25 c#3 on January 15, 1997, 5.07 days after injection, and the peak concentration of approximately 251 µg/L occurred 13.5 days after injection. The average discharge rate was 9.47 L/s. The mass recovered was estimated as 7.6 kg, which is approximately 67 percent of the injected mass.

Interpretation of the 2,6 DFBA test using the Moench (1995) dual-porosity analytical solution for radially convergent

Table 2. Selected breakthrough results and estimated transport properties from radially convergent tracer tests conducted in the Bullfrog and Tram Tuffs at the C-hole Complex, 1996 to 1997.

[DFBA, difluorobenzoic acid; µg/L, micrograms per liter; m, meter; PEST, parameter-estimation software program, Watermark Computing (1994); na, not available]

Parameter	Iodide test from UE-25 c#2 to UE-25 c#3 in Lower Bullfrog-Upper Tram interval		2,6 DFBA test from UE-25 c#2 to UE-25 c#3 in Lower Bullfrog interval		Pyridone test from UE-25 c#1 to UE-25 c#3 in Lower Bullfrog interval
Breakthrough (days)	5.07		5.07		77.0
Peak concentration (µg/L)	98		251		0.252
	Visual match	**PEST match**	**Visual match**	**PEST match**	
Longitudinal dispersivity (m)	2.6	2.52	1.9–2.4	1.83	na
Peclet number	11	11.478	12–15	15.795	na
Flow porosity, ϕ_f	0.086	0.086[a]	0.072–0.099	0.072[a]	na
GAMMA (dimensionless matrix-diffusion coefficient)	0.04	3.565×10^{-2}	0.12	0.1179	na
Storage or matrix porosity, ϕ'	0.19	0.16	0.088–0.13	0.15	na

[a]Flow porosity fixed in PEST runs to visual match values.

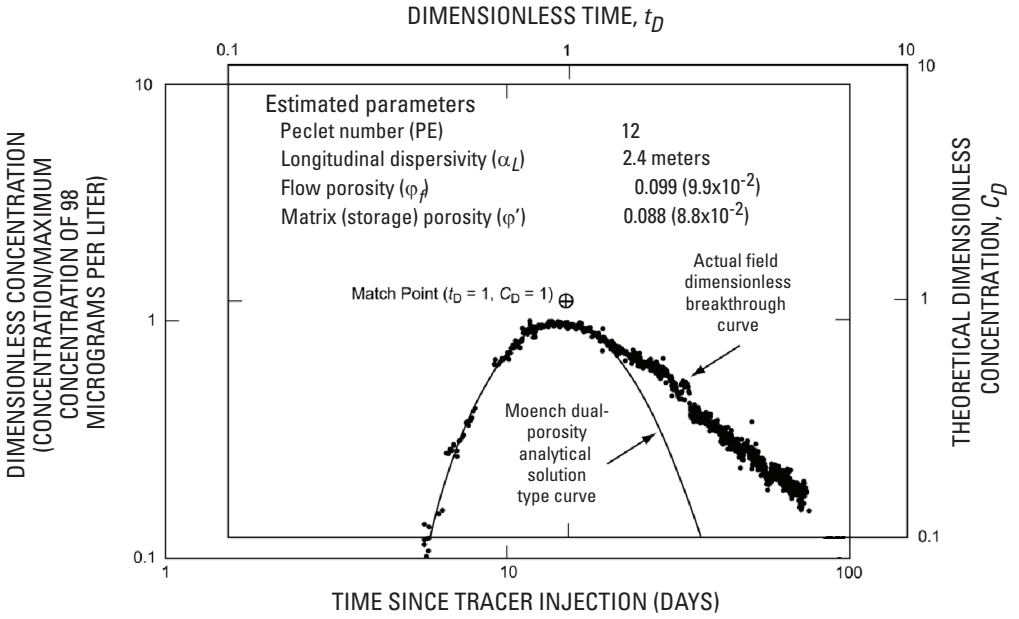

Figure 8. Visual match of the actual field breakthrough curve to the Moench (1995) dual-porosity analytical solution type curve for the 2,6 difluorobenzoic acid (DFBA) tracer test in the Lower Bullfrog interval (Matching Method 3).

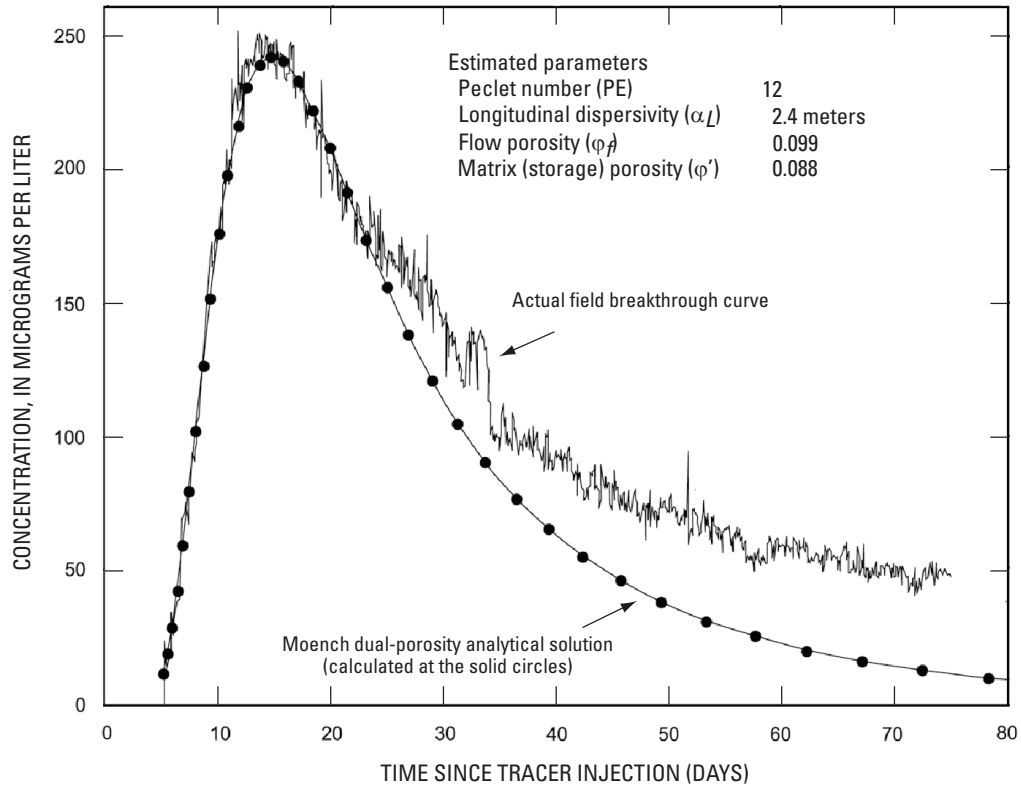

Figure 9. Visual match of the actual field breakthrough curve to the Moench (1995) dual-porosity analytical solution for the 2,6 difluorobenzoic acid (DFBA) tracer test in the Lower Bullfrog interval (Matching Method 3).

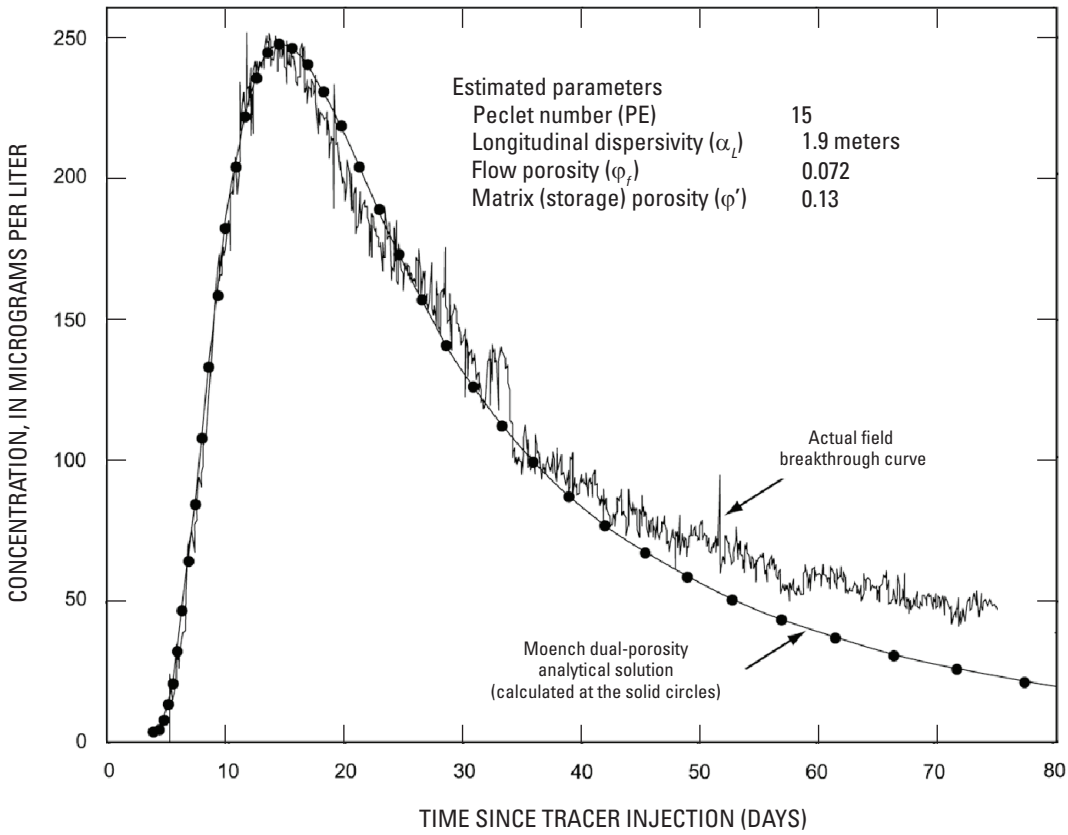

Figure 10. Visual match of the actual field breakthrough curve to the Moench (1995) dual-porosity analytical solution for the 2,6 difluorobenzoic acid (DFBA) tracer test in the Lower Bullfrog interval (Matching Method 4).

flow produced the following input parameters and results (figs. 8 and 9 use Matching Method 3 and fig. 10 uses Matching Method 4):

- discharge rate of 9.47 L/s
- aquifer thickness of 51.2 m, approximately equal to the average transmissive thickness of the Lower Bullfrog interval between boreholes UE-25 c#2 and UE-25 c#3 (fig. 3)
- Peclet number between 12 and 15 (figs. 8, 9, 10)
- advection traveltime between 12 and 16.5 days
- flow porosity between 0.072 and 0.099 (figs. 8, 9, 10)
- matrix porosity between 0.088 and 0.13 (figs. 8, 9, 10)
- longitudinal dispersivity between 1.9 and 2.4 m (figs. 8, 9, 10)

The range of values shown in figures 9 and 10 reflects two approaches for the matching process. The Peclet number of 12, flow porosity of 0.099, matrix porosity of 0.088, and a dispersivity of 2.4 m, obtained using Matching Method 3, reflect matching the rising limb of the BTC and honoring the initial decline closely (figs. 8 and 9). At longer times, the data and the match diverge, possibly indicating secondary arrivals from longer residence-time flow pathways. The approach in figure 10 is to match the rising limb of the BTC and reasonably match the complete declining portion of the curve using Matching Method 4.

The program PEST was applied to the 2,6 DFBA test results by starting with the visual graphical fit to the BTC presented in figure 10, for which PE = 15, SIGMA = 1.7, and GAMMA = 0.12. Three PEST runs were made, each with one of these parameters changed from the above values while the others were held constant. In the first run, PEST was given PE = 15, SIGMA = 3.0 (intentionally changed from its best-visual-match value of 1.7), and GAMMA = 0.12, and it was allowed to change only SIGMA. At the end of this run, PEST converged on an optimal value of SIGMA = 1.878 and an associated confidence interval for SIGMA. In the second run, PEST was given the values PE = 8 (intentionally changed from its best-visual-match value of 15), SIGMA = 1.878 and GAMMA = 0.12, and it was allowed to change only PE. At the end of this run, PEST converged on an optimal value of PE = 15.795 and an associated confidence interval for PE. In the third run, PEST was given the values PE = 15.795, SIGMA = 1.878, and GAMMA = 1.0 (intentionally changed

from its best-visual-match value of 0.12), and it was allowed to change only GAMMA. At the end of this run, PEST converged on an optimal value of GAMMA = 0.1179 and an associated confidence interval for GAMMA. These optimal values, their associated confidence intervals, and the fit to the actual BTC that they produce, are presented in figure 11.

The visual graphical match parameters and the PEST match parameters are quite close. The Peclet number and dispersivity estimates vary by approximately 5 percent as can be seen by comparing figures 10 and 11. The visual graphical match matrix-porosity estimate is between 0.088 and 0.13, and the PEST match estimate is 0.15.

Pyridone Tracer Test in the Lower Bullfrog Interval

On January 9, 1997, approximately 3.02 kg of pyridone, mixed with about 795 L of water from borehole UE-25 c#3, was injected into borehole UE-25 c#1, followed by 252 L of rinsate and chase water from UE-25 c#3 to test the Lower Bullfrog interval. This injection was made while UE-25 c#3, the production well, was being pumped at an average rate of 9.53 L/s. A total of about 2,080 L of fluid was injected, the first part of which was the fluid in the injection string

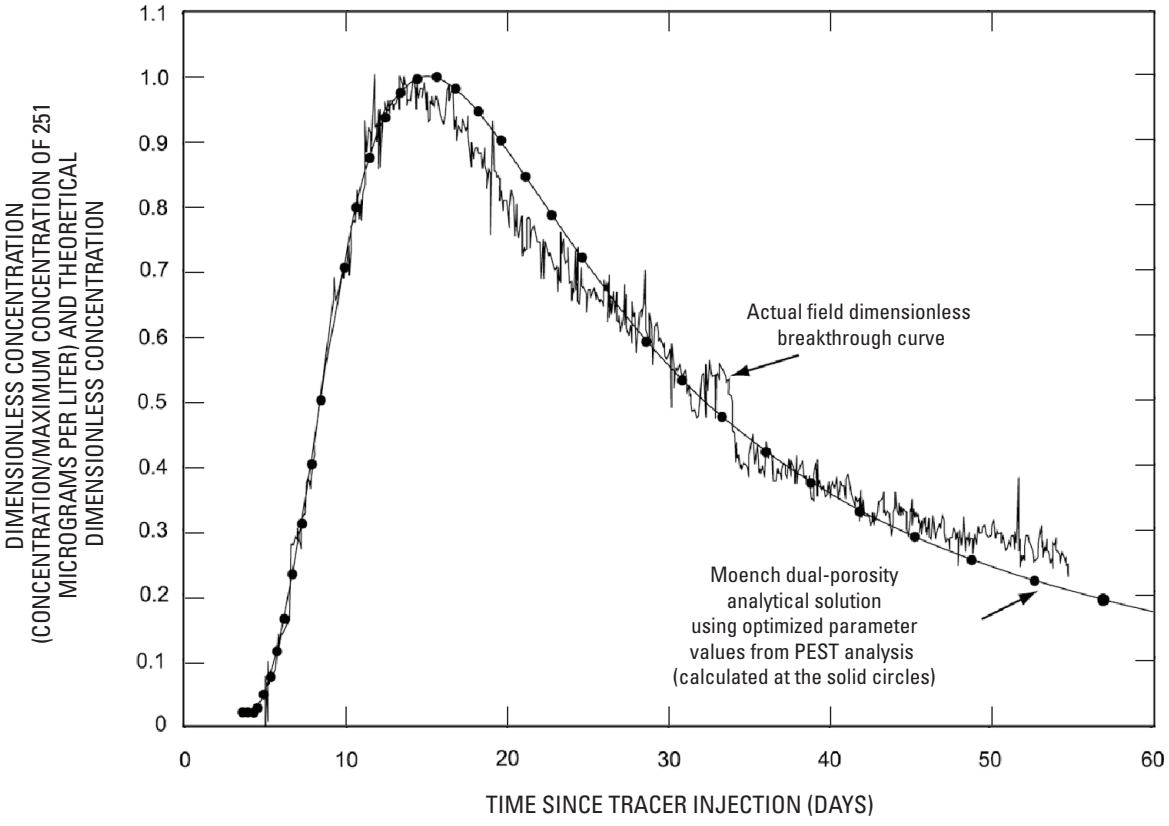

EXPLANATION

Initial parameter estimates from the visual match of these data (fig. 10)

PEST-optimized parameter results (with 95-percent confidence intervals)

Peclet number (PE)	15.795 (15.500–16.091)
Dimensionless storage coefficient (SIGMA)	1.878 (1.655–2.101)
Dimensionless diffusion coefficient (GAMMA)	0.1179 (0.01741–0.2185)
Other estimated parameters	
Longitudinal dispersivity (α_L)	1.83 meters
Flow porosity (φ_f)	0.072
Matrix (storage) porosity (φ')	0.15

Figure 11. PEST-optimized match of the actual field breakthrough curve to the Moench (1995) dual-porosity analytical solution for the 2,6 difluorobenzoic acid (DFBA) tracer test in the Lower Bullfrog interval (Matching Method 4).

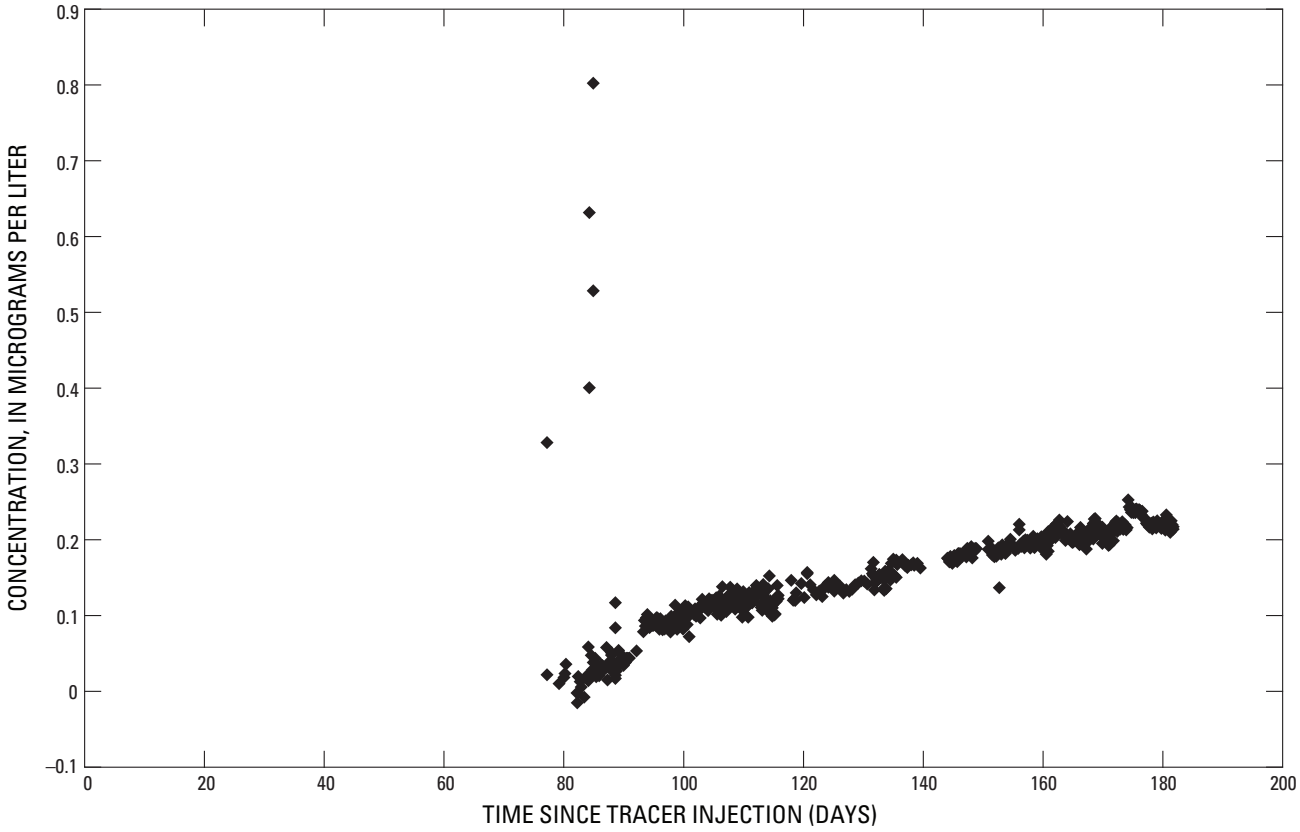

Figure 12. Breakthrough curve for the pyridone tracer test in the Lower Bullfrog interval from January 9 to July 10, 1997.

preceding the injectate solution. The average injection rate was 0.38 L/s. Chemical analysis using the HPLC method indicated that the pyridone injectate solution had an average concentration of about 3,000 mg/L (or 3×10^6 µg/L).

Breakthrough of the tracer at UE-25 c#3 occurred on March 27, 1997, 77.0 days after injection (fig. 12). The concentration of pyridone in samples continued to increase, but at a decreasing rate, and the test was terminated on November 12, 1997, before a clear peak in concentration was observed. Except for very high concentrations at the time of breakthrough (up to about 0.8 µg/L), the maximum concentration of pyridone was 0.252 µg/L, as of July 10, 1997, which was determined by analyses in the laboratory where detection limits were much lower (0.01 µg/L) than the field detection limit of 0.1 µg/L. Because the pyridone test was terminated before a peak concentration was reached, no definitive analysis of the test could be made.

Tracer Tests in the Prow Pass Tuff

Tracer tests conducted in the Prow Pass Tuff at the C-holes Complex consisted of injection of 2,4,5 trifluorobenzoic acid (TFBA) and iodide in the first test, and 2,3,4,5 tetrafluorobenzoic acid (TeFBA) in the second test. The tracers were injected into borehole UE-25 c#3 in the first test and into borehole UE-25 c#1 in the second, with borehole UE-25 c#2 as the production well for both. Parameter values obtained from the conservative tracer testing in the Prow Pass Tuff are discussed in this section (table 3).

2,4,5 Trifluorobenzoic Acid and Iodide Test from Borehole UE-25 c#3 to UE-25 c#2

On June 17, 1998, a partially recirculating conservative tracer test was initiated from borehole UE-25 c#3 to UE-25 c#2 by injecting approximately 14.8 kg of 2,4,5 trifluorobenzoic acid (2,4,5 TFBA) and 12.3 kg of iodide (in the form of 14.6 kg of sodium iodide) into the Prow Pass interval of UE-25 c#3, while UE-25 c#2 was pumped at an average rate of approximately 0.33 L/s. The concentration of 2,4,5 TFBA, as determined from HPLC analyses, was about 14,200 mg/L in the injected slug and that of sodium iodide about 14,300 mg/L. About 0.095 L/s of the approximately 0.33 L/s pumped from UE-25 c#2 was piped and continuously reinjected into the Prow Pass interval of UE-25 c#3.

Table 3. Selected breakthrough results and estimated transport properties from partially recirculating tracer tests conducted in the Prow Pass Tuff at the C-hole Complex, 1998.

[TFBA, trifluorobenzoic acid; TeFBA, tetrafluorobenzoic acid; m, meter; mg/L, milligrams per liter; na, not available; --, not applicable for single-porosity solution]

Parameter	2,4,5 TFBA & iodide test from UE-25 c#3 to UE-25 c#2[1]			2,3,4,5 TeFBA test from UE-25 c#1 to UE-25 c#2[2]
	Single-porosity, radially convergent solution (Matching Method 2)	Single-porosity, partially recirculating solution (Matching Method 2)	Dual-porosity, partially recirculating solution (Matching Method 4)	
Longitudinal dispersivity (m)	1.4	0.27	0.27	na
Peclet number	20	107	107	na
Flow porosity, ϕ_f	7×10^{-4}	4.5×10^{-4}	4.5×10^{-4}	na
GAMMA (dimensionless matrix-diffusion coefficient)	--	--	4.4×10^{-4} to 0.001	na
Storage or matrix porosity, ϕ'	--	--	0.01	na

[1]Breakthrough 1.67 days; peak concentration for TFBA, 3.81 mg/L and for iodide, 2.55 mg/L.

[2]Breakthrough 17 days; peak concentration for TeFBA, 0.10 mg/L.

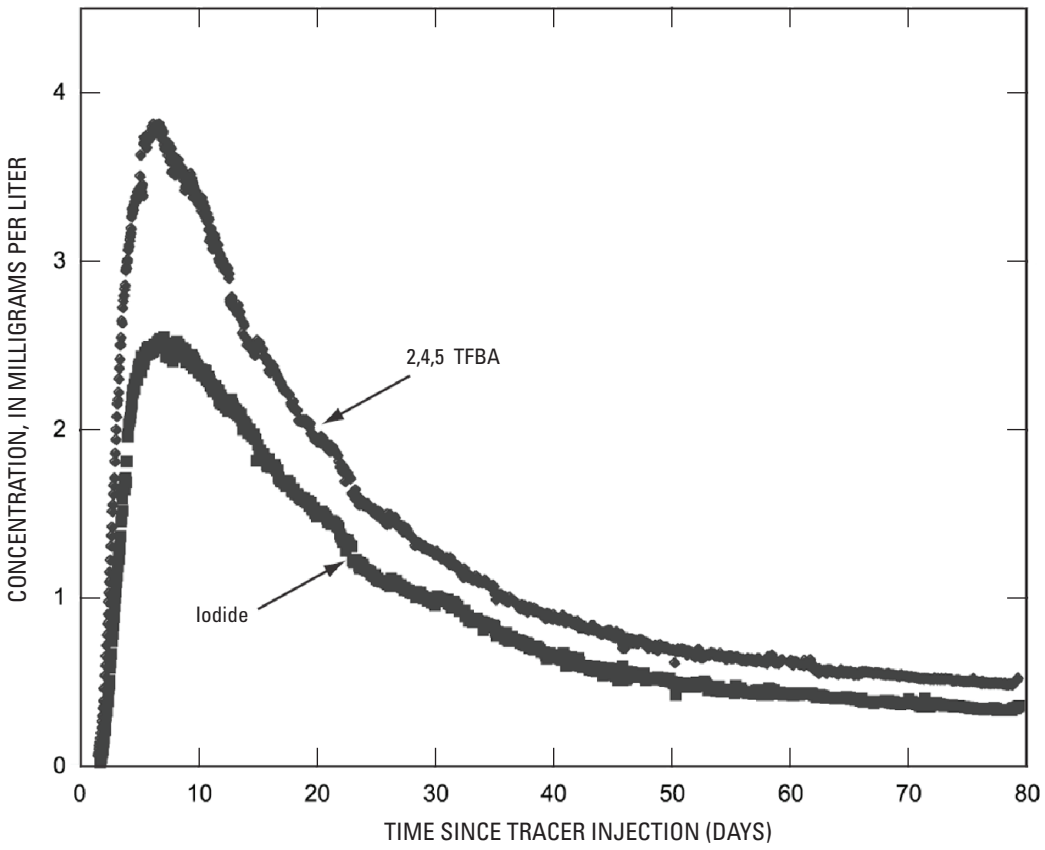

Figure 13. Actual field breakthrough curves for the partially recirculating 2,4,5 trifluorobenzoic acid (TFBA) and iodide tracer test in the Prow Pass interval.

Approximately 40 hours (1.67 days) after the injection, breakthrough of both tracers occurred in UE-25 c#2. The peak for the 2,4,5 TFBA occurred 6.74 days after injection, and the peak for iodide about 7 days after injection (fig. 13).

The 2,4,5 TFBA and iodide BTCs were analyzed using the single- and (or) dual-porosity analytical solutions of the advection-dispersion equation for a hypothetical radially convergent flow field as given in Moench (1989, 1995). These solutions also were modified by lagging and superposing to obtain the solution for the actual partially recirculating flow field. The curves were first analyzed assuming Moench's single-porosity solution for both the radially convergent and the partially recirculating flow field assumptions, using the entire curves for the fits, to obtain estimates of the flow porosity and longitudinal dispersivity for a single-porosity medium (figs. 14, 15). The curves then were analyzed assuming a dual-porosity medium and a partially recirculating flow field, also using the entire curves for the match to obtain estimates of longitudinal dispersivity, flow porosity, GAMMA, and storage porosity.

The flow porosity and longitudinal dispersivity are different for each of the solutions presented. All the solutions used the following input test-configuration parameters:

- average discharge rate of about 0.33 L/s
- recirculation rate of about 0.095 L/s
- aquifer thickness of about 61 m, the average Prow Pass thickness in UE-25 c#1 and UE-25 c#3 (calculated from Geldon and others, 2002, table 1)
- distance of about 29 m in the Prow Pass between injection and pumping wells (Geldon and others, 2002, table 1) based on borehole location at depth, not the surface
- radii of 14.0 cm for injection and pumping wells (Geldon, 1993, p. 7 and 10)
- borehole mixing length of 30.5 m (assumption discussed in the following section)

Single-Porosity, Radially Convergent Solution

The single-porosity, radially convergent solution is obtained directly from the Moench (1989) solution to the advection-dispersion equation. A best visual graphical match using the Moench single-porosity solution corresponding to flow porosity and longitudinal dispersivity values of about 7×10^{-4} and 1.4 m, respectively, is presented in figure 14, along

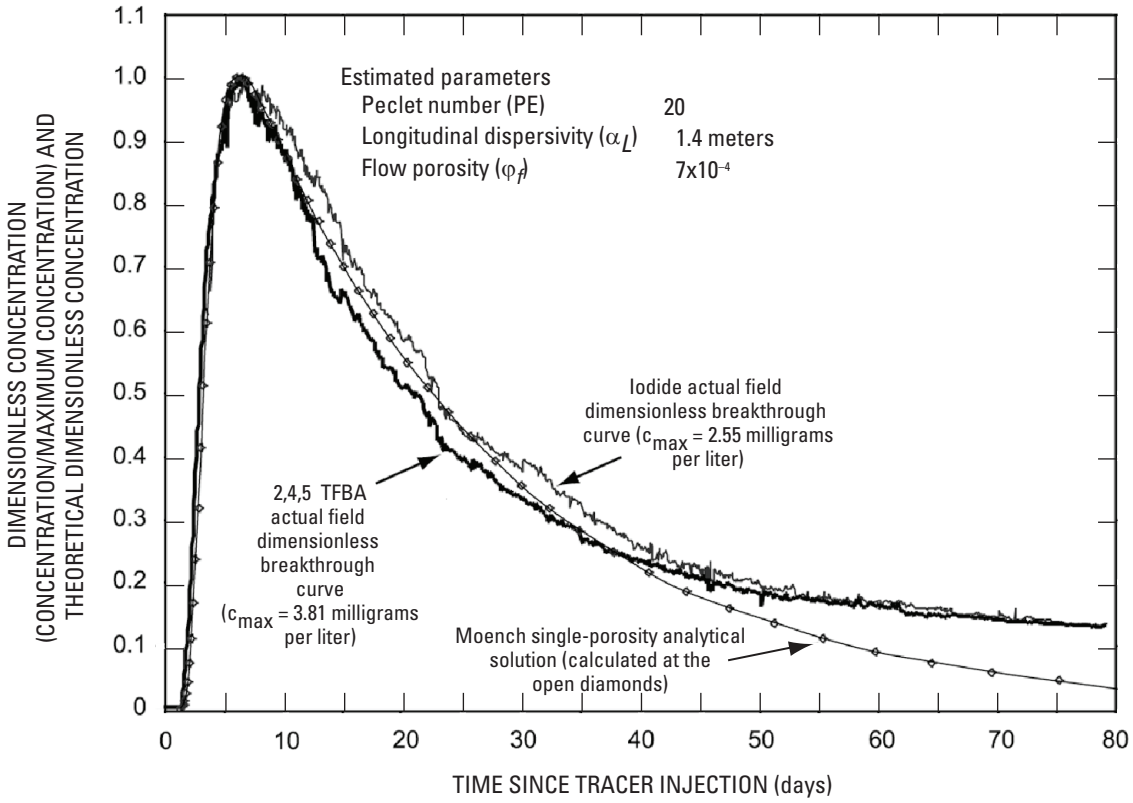

Figure 14. Visual match of the actual field breakthrough curves to the Moench (1989) single-porosity analytical solution for radially convergent flow for the 2,4,5 trifluorobenzoic acid (TFBA) and iodide tracer test in the Prow Pass interval (Matching Method 2).

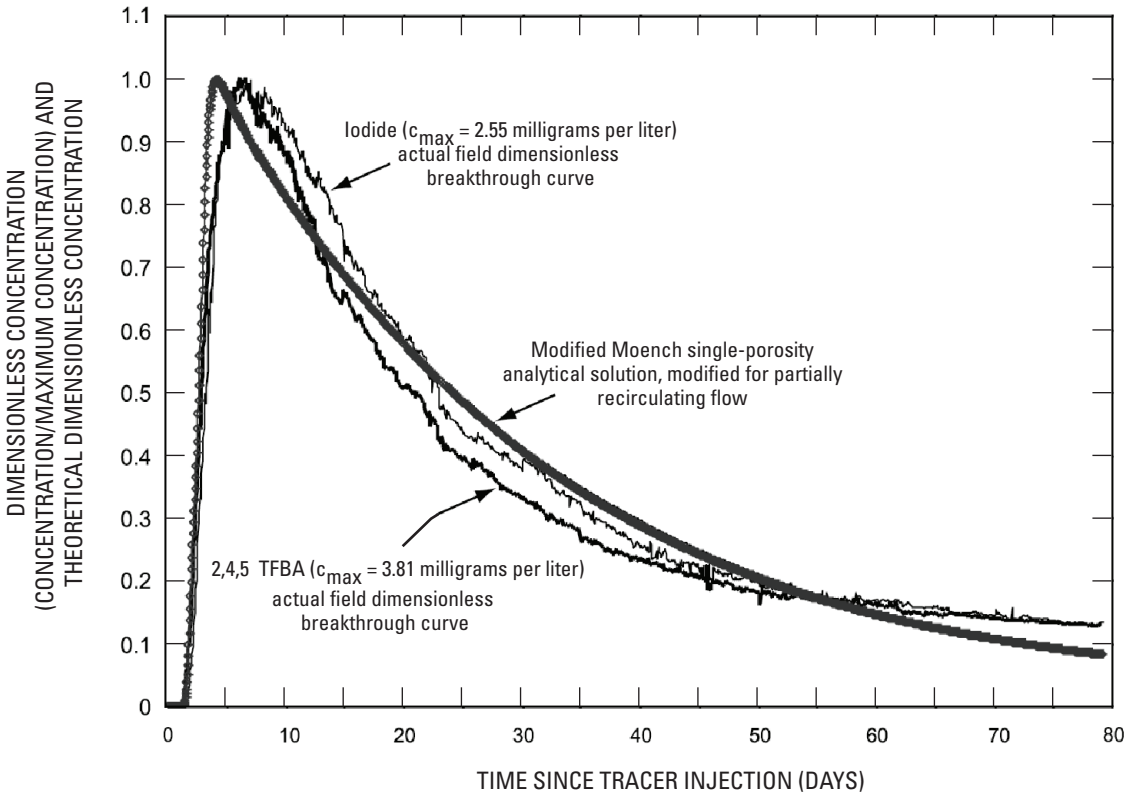

EXPLANATION

Estimated parameters	
Peclet number (PE)	107
Longitudinal dispersivity (α_L)	0.27 meter
Initial flow porosity (φ_f) (assumed for all three pathways)	4.5×10^{-4}
Three interstreamline pathways were assumed with delay factors of 2.01, 2.99, and 3.11 days	
Borehole mixing length	30.5 meters

Figure 15. Visual match of the actual field breakthrough curves to the modified Moench (1989) single-porosity analytical solution, modified for partially recirculating flow, for the 2,4,5 trifluorobenzoic acid (TFBA) and iodide tracer test in the Prow Pass interval (Matching Method 2).

with the normalized 2,4,5 TFBA and iodide BTCs. This longitudinal dispersivity value and flow length of about 29 m (flow length is equal to the distance between injection and pumping wells in a radially convergent tracer test) corresponds to a Peclet number of about 20.

The estimated longitudinal dispersivity and flow porosity values obtained from the best visual graphical match of figure 14 may be sensitive to the mixing lengths assumed for the injection and production wells. The 30.5-m mixing length assumed for all Prow Pass solutions equals the thickness of the transmissive interval within the packed-off Prow Pass interval and, as such, is consistent with the hydrogeology of the interval (Geldon and others, 2002, table 8).

The residence time of the tracer slug within the injection borehole is directly proportional to the mixing length. The concentration measured in water samples from the injection interval (obtained from an injection-interval mixing system that brought interval water to the surface and then back to the interval) rose from below detection limit to 2,721 mg/L and then back to below detection limit in 8.5 hours (Bechtel-SAIC Company, 2003, section 6.3.1.2.1.1). When the mixing length is reduced to 0.3 m and only the rising limb of the actual BTC is matched to the theoretical BTC from the single-porosity solution of Moench (1989), a longitudinal dispersivity value of about 4.3 m and a flow porosity value of 0.0016 are obtained as estimated parameters. Changing the mixing length from 30.5 m to 0.3 m constitutes a two-orders-of-magnitude change

in this parameter. Corresponding to this change in the assumed mixing length, the estimates of longitudinal dispersivity and flow porosity change from about 1.4 m and 7×10^{-4} (for a 30.5-m mixing length) to 4.3 m and 0.0016 (for a 0.3-m mixing length). This is a threefold change in longitudinal dispersivity and a twofold change in flow porosity, both less than one order of magnitude. These two estimated parameters, therefore, are not very sensitive to the mixing length.

The flow porosity value of 7×10^{-4} is within the range of 10^{-2} to 10^{-5} cited in the literature to represent fracture porosity (see, for example, Freeze and Cherry, 1979, p. 408). This implies that the flow network for this test in the Prow Pass Tuff is composed predominately of fractures.

Single-Porosity, Partially Recirculating Solution

When the radially convergent flow-field assumption of figure 14 is replaced by a partially recirculating flow field, the resulting solution to the advection-dispersion equation changes from the curve labeled "Moench single-porosity analytical solution" in figure 14 to the curve labeled "Modified Moench single-porosity analytical solution" shown in figure 15. The difference between the two solutions reflects the difference in flow-field representation and in the estimated values of longitudinal dispersivity and flow porosity used for each solution.

Two elements of partially recirculating flow are represented in this solution: the flow field and the reinjected tracer concentration. Rather than the straight streamlines converging into the pumped well for the radially convergent flow field, the partially recirculating flow-field streamlines that are within the capture zone of the pumped well emanate in all directions from the injection well but then curve around toward the pumped well (fig. 16*A*). The streamlines shown in figure 16*A* are lines of equal stream function values, where the stream function of the partially recirculating field is calculated as the sum of the stream functions of a 0.33 L/s sink (the approximate production rate) and a 0.095 L/s source (the approximate recirculation rate), about 29 m apart. The rock mass between pairs of these curved streamlines emanating from the injection well and curving toward the production well constitute distinct pathways for the tracer to take from the injection to the pumped well.

Three such interstreamline pathways emanating from the injection well and curving toward the production well (fig. 16*A*) are assumed for the partially recirculating flow analysis in this report. These pathways, labeled Interstreamline pathways 1, 2, and 3 in figure 16*A*, and the three nonlabeled pathways that are mirror images of them around the horizontal line of symmetry (Interstreamline pathway 1 and its mirror image are combined in fig. 16A), carry most of the tracer mass from injection to production well (in figure 16*A* mass leaving c#3 directly to the left [in the negative x direction] is eventually captured in c#2 after being deflected at the stagnation point [not shown] and is ignored). Symmetry allows that the analysis be restricted to only three of the six interstreamline pathways emanating from the injection well and curving toward the production well, namely Interstreamline pathways 1, 2, and 3; and that half of the mass of the tracer and half the reinjection flow rate be carried by these three pathways.

The Moench (1989) single-porosity, radially convergent solution is viewed as the solution of the advection-dispersion equation along a single straight pathway (fig. 16*B*). This solution for a particular longitudinal dispersivity value, and for a single flow porosity value that initially is assumed to apply to all three pathways (as opposed to the interpretation of three different porosity values presented later) is applied to each of the above three distinct pathways. Because the Moench solution is for a strictly convergent flow field, its application to the first-diverging-then-converging flow pattern (partially recirculating) within Interstreamline pathways 1, 2, and 3 in figure 16*A* is an approximation and will introduce some error. A delay factor (the advection traveltime calculated from the volume of rock of each pathway, the flow rate within the pathway, and the assumed porosity) is used to account for the differences in lengths, or swept volumes, of these pathways relative to the straight radially convergent pathway, and half of the injected mass is distributed among the three pathways in proportion to the flow in each of them.

The solutions from Moench (1989) for a particular longitudinal dispersivity value, an initial value of flow porosity (assumed to be the same for all three pathways), and assuming an instantaneous-slug injection are then superimposed with delay factors (previously defined) to calculate what is considered to be the system's unit response function. The summed curve represents what is seen at the pumped well in response to an instantaneous input function at the injection well in a partially recirculating flow field.

The second element of partial recirculation is that the reinjected water contains a concentration of the tracer; so, the tracer is continuously reintroduced into the aquifer. For the calculations presented here, it was estimated that this lag duration is approximately 1 hour—the estimated time of travel of the recirculated fluid in the 2.54 cm (1-inch) coil-tubing return line from the production well, c#2, to the injection well, c#3 (536 m at 5.7 L/min in Bechtel-SAIC Company, 2003, section 6.3.1.2.1.2). The injection concentration curve is then convolved (Levenspiel, 1972) with the unit response function to produce the calculated BTC for the partially recirculating flow field at the pumped well. This calculated BTC is then compared visually to the actual BTC to evaluate the goodness of the flow porosity and longitudinal dispersivity values assumed. Different values of flow porosity and longitudinal dispersivity are tried until the visual difference between calculated and actual BTCs is minimized. The values resulting in the minimum difference between the two curves are called the "optimal" values of this qualitative, visual, trial-and-error parameter-estimation process.

Using this process, a longitudinal dispersivity of 0.27 m (PE about 107) and an initial flow porosity of 4.5×10^{-4} assumed to be the same for all three pathways, which result

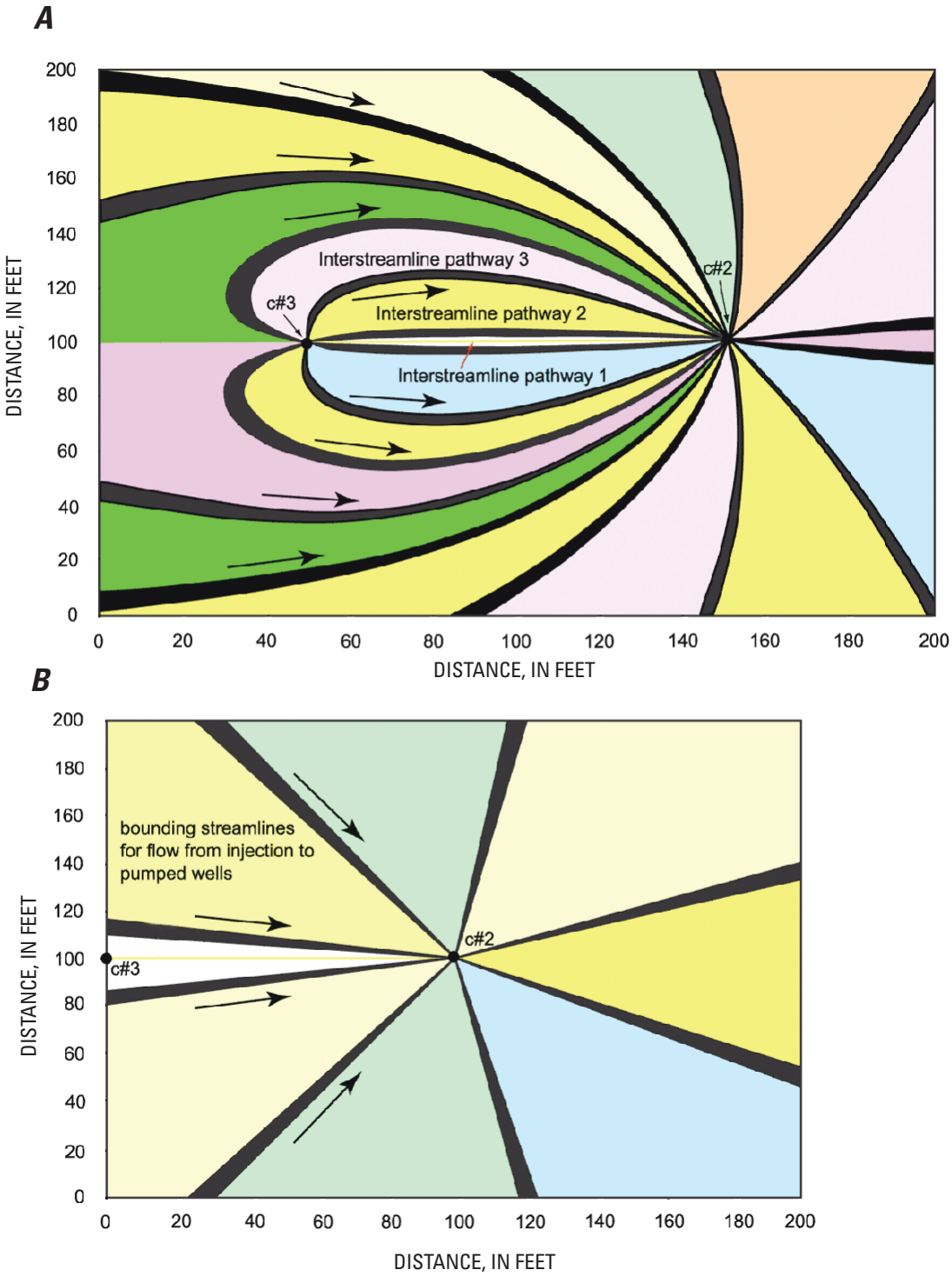

Figure 16. Comparison of ground-water streamlines around UE-25 c#2 (production well) and UE-25 c#3 (injection well) for: (*A*) partially recirculating flow field; (*B*) radially convergent flow field.

in the calculated partially recirculating BTC presented in figure 15, were obtained as the "optimal" parameters for the single-porosity, partially recirculating case (as opposed to the 1.4 m and 7×10^{-4} optimal values estimated for the single-porosity, radially convergent solution).

The delay factors for the three interstreamline pathways inherent in the calculation of the BTC of figure 15 were initially assumed to be 1.83 days for the first pathway, 3.5 days for the second, and about 7.5 days for the third. (These are the advection traveltimes calculated from the volume of rock of each pathway, the assumed same initial porosity value for all three pathways, and the flow rate within each pathway.) However, use of these delay factors produced a calculated BTC that did not fit the actual BTC. The fit was substantially improved by changing the delay factors to 2.01 days, 2.99 days, and 3.11 days, which resulted in the calculated BTC of figure 15. Because these three delay factors are not the ones indicated by the volumes of rock calculated for the three interstreamline pathways, they are interpreted to represent the uncertainty in either the same initial flow-porosity value assumed for all three pathways or in the assumed streamline pattern and resulting rock volumes. If the streamline pattern with associated rock volumes is assumed correct, then the delay factors of 2.01, 2.99, and 3.11 days correspond to flow porosities of about 0.0005, 0.0004, and 0.0002 for the three interstreamline pathways, respectively. However, because different porosities for the three pathways is not compatible with the underlying homogeneity assumption, the three porosities provide a range of uncertainty for the single porosity estimate of 4.5×10^{-4} used for all partially recirculating cases.

The results shown in figures 14 and 15 indicate that if the BTCs of 2,4,5 TFBA and iodide are analyzed as if they result from a radially convergent flow field, ignoring that the real flow field is partially recirculating, some error in the estimated parameters occurs. A longitudinal dispersivity of about 1.4 m is obtained when radially convergent conditions are assumed, approximately 5 times the 0.27 m obtained when the partially recirculating flow field is recognized. The flow porosity of about 7×10^{-4} obtained for radially convergent conditions is about 1.6 times the initial flow porosity of 4.5×10^{-4} obtained for partially recirculating conditions.

The partially recirculating solution shown in figure 15 (and other tests in the Prow Pass Tuff section) does not match the actual BTCs as well as the radially convergent solution of figure 14, even though the latter ignores the flow field created by partial recirculation. This could mean either that the explicit representation of the partially recirculating flow field is not important and that the test can be analyzed successfully as a radially convergent tracer test, or that the homogeneous and isotropic representation of the partially recirculating flow field presented here does not represent the actual partially recirculating flow field very well. Perhaps increasing the number of the interstreamline pathways beyond three to, in effect, "discretize" the flow field more finely would improve the matches. A fourth interstreamline pathway capturing the ignored mass between interstreamline pathway 3 and the stagnation point may improve the matches.

Dual-Porosity, Partially Recirculating Solution

The calculated dual-porosity, partially recirculating solution uses the same parameter values as the single-porosity, partially recirculating solution presented: a longitudinal dispersivity of 0.27 m and the same initial flow porosity value of 4.5×10^{-4} for all three pathways. Two calculated BTCs obtained for a matrix (storage) porosity of 0.001 and two dimensionless matrix-diffusion coefficients (GAMMA) of 4.4×10^{-4} and 0.001, are presented in figure 17, along with the actual BTCs of 2,4,5 TFBA and iodide.

The effect of changing GAMMA on the shape of the falling limb of the theoretical BTC depends on the matrix (storage) porosity. For two tracers traveling in the same medium under the same testing configuration, the ratio of the dimensionless matrix-diffusion coefficient, GAMMA, for the two tracers is the same as the ratio of their free-water molecular diffusion coefficients (Moench, 1995, table 1). The free-water molecular diffusion coefficients of 2,4,5 TFBA and iodide are 8.0×10^{-6} cm^2/s and 18×10^{-6} cm^2/s, respectively (Bowman, 1984, table 2; Skagius and Neretnieks, 1986, tables 2 and 3), which corresponds to a ratio of 8/18 or 1:2.25 (TFBA: iodide). GAMMA values of about 4.4×10^{-4} and 0.001 were chosen for figure 17 because they provide the best visual match for the BTCs in the figure and have the 1:2.25 ratio.

Figure 17 shows the effects on matrix diffusion, as represented by the two calculated BTCs, of changing GAMMA by a factor of 2.25 for a fixed matrix (storage) porosity of 0.001 and the fixed flow rate of the test. The effect of increasing the free-water molecular diffusion coefficient, which increases GAMMA, causes a delay of the calculated BTC for higher GAMMA relative to the BTC for lower GAMMA. This "differential matrix-diffusion delay" is seen as a horizontal offset between the two calculated BTCs in figure 17. The larger the difference in GAMMA between the two curves, the larger the differential matrix-diffusion delay.

Furthermore, the differential matrix-diffusion delay for a particular pair of free-water molecular diffusion coefficients (or GAMMA values) increases with increasing matrix (storage) porosity. Figure 18, which uses the same pair of GAMMA values used in figure 17, shows that when the storage porosity is increased from the 0.001 value of figure 17 to 0.01, the differential matrix-diffusion delay is markedly larger.

The differential matrix-diffusion delay between calculated BTCs in figure 18 is similar to that between the actual BTCs for 2,4,5 TFBA and iodide, and this indicates a storage porosity value of approximately 0.01. This result is combined with earlier ones to indicate a dual-porosity medium with an

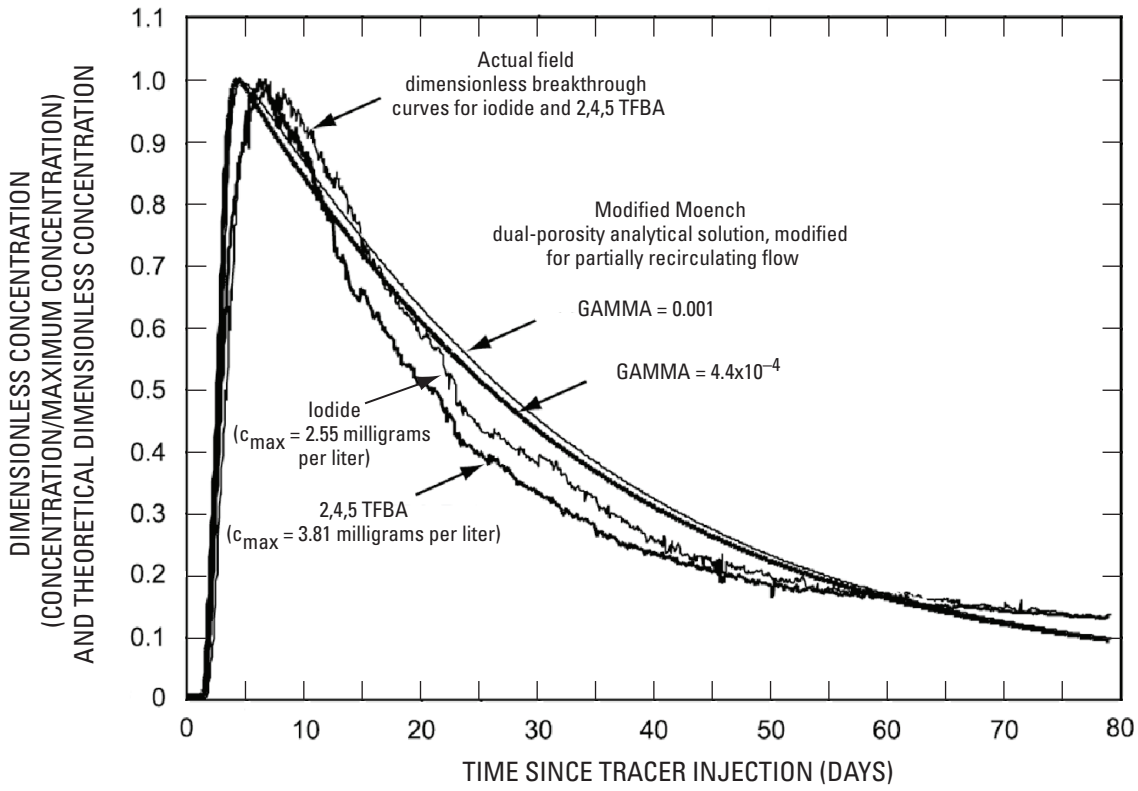

EXPLANATION

Estimated parameters	
Peclet number (PE)	107
Longitudinal dispersivity (α_L)	0.27 meter
Initial flow porosity (φ_f) (assumed for all three pathways)	4.5×10^{-4}
Other estimated parameters	
Storage porosity	0.001
Dimensionless diffusion coefficient (GAMMA)	4.4×10^{-4} and 0.001
Three interstreamline pathways were assumed with delay factors of 2.01, 2.99, and 3.11 days	
Borehole mixing length	30.5 meters

Figure 17. Visual match of the actual field breakthrough curves to the modified Moench (1995) dual-porosity analytical solution, modified for partially recirculating flow, for the 2,4,5 trifluorobenzoic acid (TFBA) and iodide tracer test in the Prow Pass interval showing effects of changing GAMMA, with a storage porosity of 0.001 (Matching Method 4).

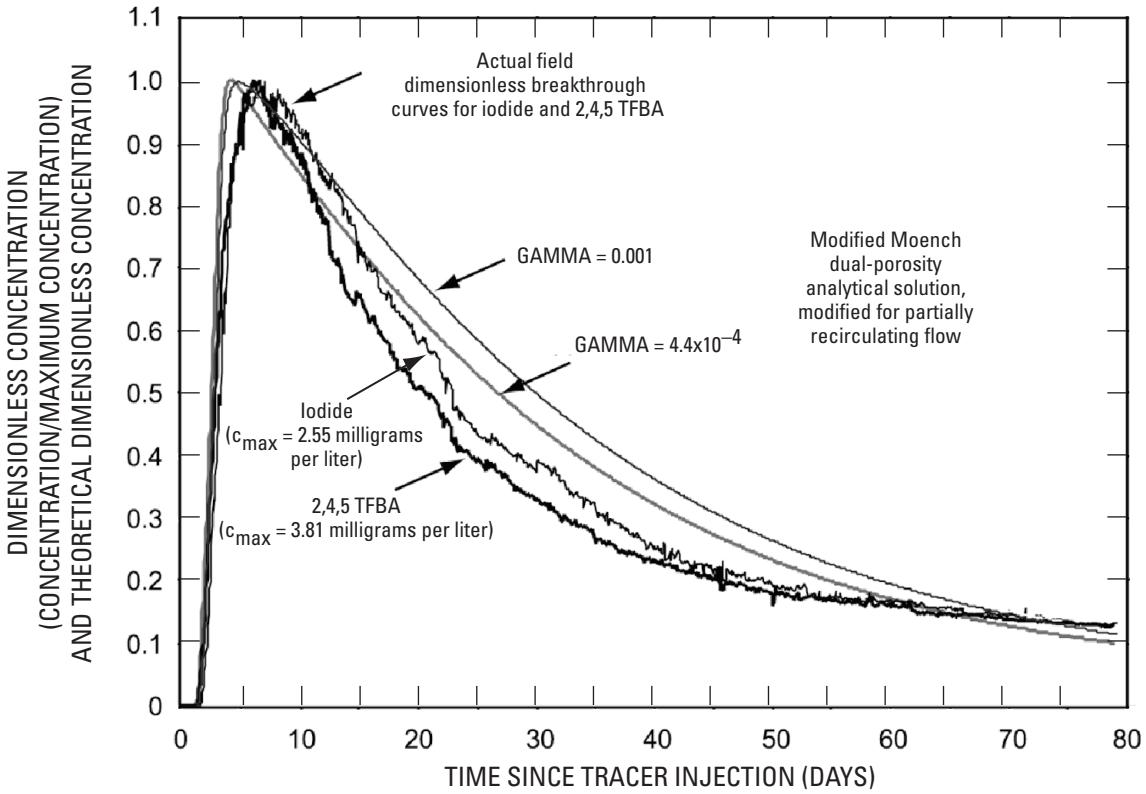

EXPLANATION

Estimated parameters	
Peclet number (PE)	107
Longitudinal dispersivity (α_L)	0.27 meter
Initial flow porosity (φ_f) (assumed for all three pathways)	4.5×10^{-4}
Other estimated parameters	
Storage porosity	0.01
Dimensionless diffusion coefficient (GAMMA)	4.4×10^{-4} and 0.001
Three interstreamline pathways were assumed with delay factors of 2.01, 2.99, and 3.11 days	
Borehole mixing length	30.5 meters

Figure 18. Visual match of the actual field breakthrough curves to the modified Moench (1995) dual-porosity analytical solution, modified for partially recirculating flow, for the 2,4,5 trifluorobenzoic acid (TFBA) and iodide tracer test in the Prow Pass interval showing effects of changing GAMMA, with a storage porosity of 0.01 (Matching Method 4).

initial flow porosity of 4.5×10^{-4} (which may represent three interstreamline pathways of flow porosities ranging from 0.0002 to 0.0005), a storage porosity of 0.01, and a longitudinal dispersivity of 0.27 m.

2,3,4,5 Tetrafluorobenzoic Acid Test from Borehole UE-25 c#1 to UE-25 c#2

On July 31, 1998, the conservative tracer 2,3,4,5 tetrafluorobenzoic acid (2,3,4,5 TeFBA) was injected in the Prow Pass interval of borehole UE-25 c#1 while UE-25 c#2 continued to be pumped at the average rate of approximately 0.33 L/s with no recirculation. Breakthrough of this tracer at UE-25 c#2 occurred on August 14, 1998, 13.2 days after injection, and the concentration eventually rose to a maximum of about 0.10 mg/L approximately 65 days after tracer injection (fig. 19). The accentuated peak shown in figure 19 is a result of a disturbance in borehole UE-25 c#2 in which the pump stopped and had to be restarted on September 22, 1998, approximately 53 days after injection. The results of this tracer test were used to qualitatively assess flow heterogeneity at the C-wells (see Bechtel-SAIC Company, 2003, table 6.3–1).

Summary of Transport Parameter Values and Presentation of Conceptual Models of Solute Transport in the Bullfrog, Tram, and Prow Pass Tuffs

Estimated transport parameter values varied among the tracer tests in the Bullfrog, Tram, and Prow Pass Tuffs. Conceptual models of solute transport consistent with these parameter estimates are different for the Bullfrog-Tram and Lower Bullfrog intervals than they are for the Prow Pass interval. Variations in the values of longitudinal dispersivity, flow porosity, and matrix (storage) porosity result from physical processes, such as the scale-dependence of dispersivity (when comparing tracer tests conducted from borehole UE-25 c#1 to those conducted between boreholes UE-25 c#2 and UE-25 c#3), as well as from variability in the

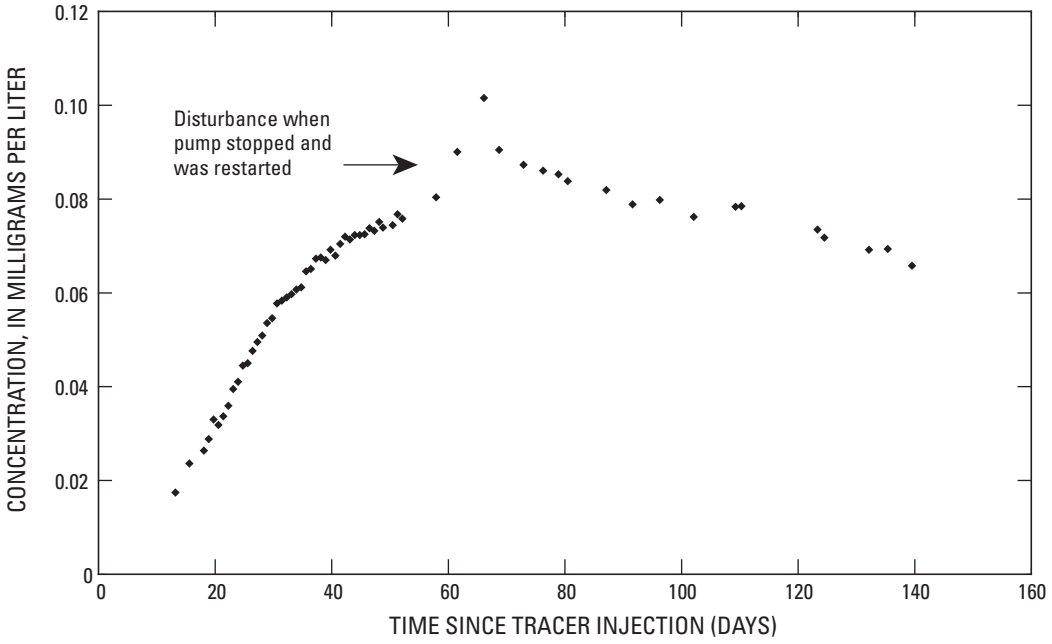

Figure 19. Actual field breakthrough curve for the 2,3,4,5 tetrafluorobenzoic acid (TeFBA) tracer test in the Prow Pass interval.

transport characteristics of the tracer materials. However, there is good agreement in dispersivity values obtained from tracer tests conducted between boreholes UE-25 c#2 and UE-25 c#3 in the Bullfrog and Tram intervals. Peclet numbers derived from the tests are similar, ranging from approximately 11 to 15.8; therefore, the longitudinal dispersivities also are similar, ranging from about 2.6 m to 1.83 m, respectively (table 2).

The breakthrough times of 5.07 days are identical for the iodide and the 2,6 DFBA tracer tests (table 2), and the advection traveltimes are within 12 percent. The inferred flow porosities are similar, which implies that similar flow pathways are used by the tracers in those tests.

The parameter estimates are robust (not sensitive to the matching method) because the visual graphical match is similar to the PEST match. The differences are less than 5 percent for all parameters except matrix porosity, and matrix porosity estimates vary by 0.02 (13 percent) for the Lower Bullfrog tracer test and 0.03 (16 percent) for the Bullfrog-Tram tracer test.

The higher-than-expected estimated flow porosities for the Bullfrog and Tram Tuffs of 0.086 and 0.072 to 0.099 (table 2) indicate that the pathways between boreholes UE-25 c#2 and UE-25 c#3 in these intervals are not connected well. Test results using microspheres (Bechtel-SAIC Company, 2003, sections D3 and D4) are consistent with this interpretation. The arrival of the microspheres at the recovery borehole demonstrates the existence of a connected pathway, with an aperture at least 0.36 micrometer wide. The small recovery percentage of the microspheres, however, also suggests poorly connected/tortuous pathways, dead-ended flow pathways, or some attachment mechanism.

The estimates of flow porosity cannot be separated from the parameter h, which represents a uniform thickness. In conducting tracer tests in isolated, permeable intervals in fractured rock, identification of a meaningful thickness is difficult because transport occurs through an interconnected network of fractures. For this report, the appropriate thickness was based either on the interval thickness or the transmissive thickness according to Geldon and others (2002, tables 1 and 8, respectively). For the 56-m- to 73-m-thick Prow Pass interval, the appropriate thickness was assumed to be the interval thickness and for the 94-m- to 116-m-thick Lower Bullfrog interval and the 168-m- to 180-m-thick Bullfrog-Tram interval, it was assumed to be the transmissive thickness.

If the ratio of advection traveltimes is equal to the ratio of first arrivals (which is strictly correct only for purely advection flow without dispersion), then equation 1 shows that, for the same pumping rate, q_o; aquifer thickness, h; and flow porosity, ϕ_f; and ignoring r_w relative to r_L, the ratio of first arrivals is equal to the ratio of squares of the interborehole distances. For the pyridone and 2,6 DFBA tests, the ratio of first arrivals, 15.2 (77.0 d/5.07 d), is within one order of magnitude of 8.54, the ratio of the squares of the interborehole distances of UE-25 c#1 to UE-25 c#3 and UE-25 c#2 to UE-25 c#3, $(85.6\text{ m})^2/(29.3\text{ m})^2$ (Geldon and others, 2002, table 1).

Tracer testing in the Prow Pass interval (table 3) shows different transport characteristics than those obtained in the Bullfrog and Tram intervals. The flow porosity was found to be 0.00045 in the Prow Pass as opposed to 0.072 to 0.099 in the Bullfrog and Tram intervals (tables 3 and 2, respectively). This difference indicates that the flow network in the Prow Pass is dominated by interconnected fractures (fracture porosity is in the range from 10^{-2} to 10^{-5}), whereas in the Bullfrog and Tram intervals, the flow network is dominated by discontinuous fractures with interconnecting segments of matrix (figs. 4 and 20).

Longitudinal dispersivity in the Prow Pass Tuff testing at the scale of the distance between UE-25 c#2 and UE-25 c#3 is calculated as 0.27 m, whereas it is 1.9 to 2.6 m in the Bullfrog and Tram intervals at the same scale. A relatively small dispersivity is consistent with a flow network dominated by interconnected fractures (Prow Pass), and a relatively large dispersivity is consistent with a flow network dominated by discontinuous fractures with interconnecting segments of matrix (Bullfrog and Tram). The more the actual microscopic flow pathways are different from the macroscopic, averaged, flow pathway, the larger the longitudinal dispersivity. A flow network dominated by discontinuous fractures with interconnecting segments of matrix (Bullfrog and Tram) will have more microscopic flow pathways than a flow network dominated by interconnected fractures (Prow Pass).

The storage (or matrix) porosity calculated for the Prow Pass Tuff is 0.01 (table 3), whereas it is 0.088 to 0.19 for the Bullfrog and Tram (table 2). A small storage porosity is consistent with a dual-porosity medium dominated by interconnected fractures (Prow Pass). In such a medium, the storage component, which is assumed to consist of dead-end fractures and the part of the matrix not contributing to the flow network, would be dominated by fractures that have very small porosities. Similarly, a large storage porosity is consistent with a dual-porosity medium dominated by discontinuous fractures with interconnecting segments of matrix (Bullfrog and Tram). In such a medium, the porosity of the storage component (dead-end fractures and the part of the matrix not contributing to the flow network) would be dominated by the large porosity of the matrix component of storage.

Uncertainties and Limitations

Several factors contributed to uncertainty in, and limitations of, tracer-test results and interpretations. During the iodide tracer test in the Bullfrog-Tram interval (February to March 1996), the pump gradually failed, leading to a decreasing flow rate during the test, which changed from 8.5 L/s at the beginning of the test to 6.2 L/s at the end of the test (Bechtel-SAIC Company, 2003, section 6.3.5.1). This violated the assumption of a steady-state flow field in the Moench (1989, 1995) analytical methods used to analyze tracer test results, which would introduce some error into estimates of

<table>
<tr><th colspan="3">Equivalent porous medium (EPM)</th><th colspan="2">Bullfrog-Tram and Lower Bullfrog intervals</th><th colspan="2">Prow Pass interval</th></tr>
<tr><td rowspan="4">Flowing water component</td><td rowspan="5">porosity</td><td rowspan="4">Single porosity</td><td>Low ϕ_f</td><td>Interconnected fractures</td><td rowspan="2">Low flow porosity, ϕ_f</td><td rowspan="2">Interconnected fractures</td></tr>
<tr><td rowspan="3">High flow porosity, ϕ_f</td><td>Discontinuous fractures carrying moving water</td></tr>
<tr><td rowspan="2">Matrix allows flow between close discontinuous fractures carrying moving water</td><td rowspan="2">High ϕ_f</td><td>Discontinuous fractures carrying moving water</td></tr>
<tr><td>Matrix allows flow between close discontinuous fractures carrying moving water</td></tr>
<tr><td rowspan="3">Immobile water component (storage)</td><td>Low ϕ'</td><td>Discontinuous fractures (dead-end fractures): stagnant water</td><td rowspan="2">Low matrix porosity, ϕ'</td><td rowspan="2">Discontinuous fractures (dead-end fractures): stagnant water</td></tr>
<tr><td>High matrix porosity, ϕ'</td><td>Matrix No close fractures with moving water for the matrix to connect</td></tr>
<tr><td>High ϕ'</td><td>Matrix No close fractures with moving water for the matrix to connect</td></tr>
</table>

Figure 20. Conceptual diagram comparing the proportions of the flowing and immobile water components of the fractured rock equivalent porous mediums (EPMs) in the Bullfrog-Tram and Prow Pass intervals at the C-hole Complex.

flow porosity. This source of uncertainty was eliminated for subsequent tests by replacing the pump.

There was uncertainty regarding the extent to which the tracer was evacuated from the borehole to the aquifer in the injection interval during the Bullfrog-Tram and Lower Bullfrog tests. This problem was due to the thickness of the injection intervals (97 m for the Lower Bullfrog, and about 170 m for the Bullfrog-Tram interval) and to the lack of downhole mixing. Attempts were made to reduce this source of uncertainty in the Prow Pass testing by reducing the injection-interval thickness and by designing and deploying a downhole system capable of mixing the tracer after its injection into the borehole. Even though the downhole mixing system worked only marginally, it is believed that the above two combined measures did minimize stratification of tracer concentration in the borehole and led to better evacuation of the tracer into the aquifer.

The influence of the natural potentiometric head gradient to the southeast that exists at the C-holes (Luckey and others, 1996, figs. 8 and 9) on tracer recovery at the pumped well is a source of uncertainty. Determination of the capture zone of the pumped well and how it is altered by the existence of a natural gradient depend on the assumptions made regarding heterogeneity and anisotropy of hydrogeologic parameters. Tracer mass that was not recovered by the pumped well is evidence that pathways other than the postulated radially convergent or partially recirculating streamlines toward the pumped well (fig. 16) contribute to the transport of tracers.

When analyzing tracer test results using an analytical solution to the advection-dispersion equation, such as the Moench (1989, 1995) solutions used in this study, several assumptions are made, as mentioned previously. The medium is assumed to be homogeneous and isotropic, and the flow regime is assumed to be strictly areal (that is, no vertical component). On the basis of these assumptions, transport parameters are determined by matching type curves to the BTCs. To the extent that any of these assumptions are not correct for the tracer tests presented in this report, some uncertainty in the estimated parameters is introduced.

When assuming a dual-porosity medium, as was done in this study, the number of transport parameters that would have to be determined is large, and nonuniqueness of the solution becomes an issue. The uncertainty was reduced by using the PEST quantitative parameter-estimation software (Watermark Computing, 1994). PEST quantifies uncertainties in parameter determinations by providing confidence intervals on optimal parameter values that it produces. PEST was used to quantify parameter uncertainty for two of the three radially convergent conservative tracer tests conducted in the Bullfrog and Tram intervals.

A limitation of all tracer tests conducted so far is that they produce estimates of only longitudinal dispersivity, not transverse dispersivity. Transverse dispersivity represents the medium's ability to disperse a solute in a direction perpendicular to streamlines. In addition, in all tracer tests, the estimation of flow porosity has the uncertainty of an unknown travel distance between the tracer injection and production wells. The probability that the travel distance is a straight line distance is remote. The unknown travel distance can affect the flow porosity calculation.

Uncertainty in the chemistry data is presented in terms of the error bounds that bracket the data. For the tracer concentrations, the maximum error is plus or minus 10 percent of the value as was discussed under "Field and Laboratory Methods." These limitations are a function of the HPLC analytical technique used to obtain tracer concentrations.

Summary

Tracer tests were conducted among three boreholes (UE-25 c#1, UE-25 c#2, UE-25 c#3) known as the C-hole Complex to determine the hydraulic and chemical-transport characteristics of the underlying rocks in order to evaluate the potential for transport of radionuclides from a proposed high-level nuclear-waste repository at Yucca Mountain, Nevada.

The C-holes are completed in a sequence of Miocene tuffaceous rocks that are covered by Quaternary alluvium. The tuffaceous rocks are estimated to be 1,040 to 1,590 m thick in the vicinity of the C-holes, where they consist of nonwelded to densely welded ash-flow tuff with intervals of ash-fall tuff and volcaniclastic rock. The lower part of the tuffaceous-rock sequence includes the Prow Pass, Bullfrog, and Tram Tuffs of the Crater Flat Group. The rocks are pervaded by tectonic and cooling fractures that strike predominantly north-northeast to north-northwest and dip westward at angles of 50 to 87 degrees. Paleozoic limestone and dolomite that underlie the tuffaceous rocks are estimated to be about 455 m below the bottom of the C-holes.

Conservative tracer tests (four radially convergent and one partially recirculating) were conducted at the C-hole Complex from February 1996 to September 1998 to establish flow porosity, storage porosity, longitudinal dispersivity, and extent of matrix diffusion in the Bullfrog and Tram Tuffs and the Prow Pass Tuff. Multiple cross-hole tests were conducted, and multiple solutions were used to interpret the results.

All tracer tests were analyzed by applying the Moench single- or dual-porosity analytical solutions to the advection-dispersion equation or by superposition of these solutions. This multiple-analysis approach was done to ensure that the appropriate solution method is used in matching a particular set of data.

Nonlinear regression techniques in the form of a parameter-estimation software program (PEST) were used to supplement the analyses conducted using the Moench single- and dual-porosity solutions. PEST was used to corroborate tracer solution results, to obtain optimal parameter values from the solutions, and to quantify parameter uncertainty resulting from analyzing two of the three radially convergent conservative tracer tests conducted in the Bullfrog and Tram intervals.

Analysis of the tracer-test data in the Bullfrog Tuff and Tram Tuff resulted in longitudinal dispersivity values ranging from 1.83 to 2.6 m, flow-porosity values ranging from 0.072 to 0.099 and matrix-porosity values ranging from 0.088 to 0.19. The parameter estimates are robust (not sensitive to the matching method) because the visual graphical match is similar to the PEST match, both of which are based on the dual-porosity analytical solution.

The higher-than-expected flow-porosity values obtained for the Bullfrog and Tram Tuffs indicate that the pathways between boreholes UE-25 c#2 and UE-25 c#3 in these intervals are not connected well. Independent test results using microspheres are consistent with this interpretation.

Analysis of the tracer-test data in the Prow Pass Tuff resulted in a longitudinal dispersivity of 0.27 m, a flow porosity of 4.5×10^{-4}, and a matrix porosity of 0.01. Tracer testing in the Prow Pass interval indicates different transport characteristics than those obtained in the Bullfrog and Tram intervals. This difference indicates that the flow network in the Prow Pass is dominated by interconnected fractures, whereas in the Bullfrog and Tram, the flow network is dominated by discontinuous fractures with interconnecting segments of matrix.

Several factors contributed to uncertainty in, and limitations of, tracer-test results. These factors include equipment failure during testing, possible incomplete tracer evacuation from the injection interval, the influence of the natural potentiometric gradient, assumptions inherent in the analytical methods, and potential errors in chemical analyses.

References

Anderman, E.R., and Hill, M.C., 1999, A new multistage groundwater transport inverse method—Presentation, evaulation, and implications: Water Resources Research, v. 35, no. 4, p. 1053–1063.

Bechtel-SAIC Company, 2003, Saturated zone in-situ testing: Las Vegas, Nevada, Bechtel-SAIC Company, ANL-NBS-HS-000039 REV 00, accessed September 5, 2007, at *http://www.osti.gov/bridge*; search for report number.

Bowman, R.S., 1984, Evaluation of some new tracers for soil water studies: Journal of the Soil Society of America, v. 48, p. 987–993.

Carr, M.D., Waddell, S.J., Vick, G.S., Stock, J.M., Monsen, S.A., Harris, A.G., Cork, B.W., and Byers, F.M., Jr., 1986, Geology of drill hole UE-25 p#1—A test hole into pre-Tertiary rocks near Yucca Mountain, southern Nevada: U.S. Geological Survey Open-File Report 86–175, 87 p.

Day, W.C., Potter, C.J., Sweetkind, D.S., Dickerson, R.P., and San Juan, C.A., 1998, Bedrock geologic map of the central block area, Yucca Mountain, Nevada: U.S. Geological Survey Miscellaneous Investigations Map I–2601, scale 1:6,000.

Fahy, M.F., 1997, Dual-porosity analysis of conservative tracer testing in saturated volcanic rocks at Yucca Mountain in Nye County, Nevada: International Journal of Rock Mechanics and Mining Science, v. 34, nos. 3–4, paper 074.

Freeze, R.A., and Cherry, J.A., 1979, Groundwater: Englewood Cliffs, N.J., Prentice-Hall, 604 p.

Frizzell, V.A., Jr., and Shulters, Jacqueline, 1990, Geologic map of the Nevada Test Site, southern Nevada: U.S. Geological Survey Miscellaneous Investigations Map I–2046, scale 1:100,000.

Geldon, A.L., 1993, Preliminary hydrogeologic assessment of boreholes UE-25c #1, UE-25c #2, and UE-25c #3, Yucca Mountain, Nevada: U.S. Geological Survey Water-Resources Investigations Report 92–4016, 85 p.

Geldon, A.L., 1996, Results and interpretation of preliminary aquifer tests in boreholes UE-25c #1, UE-25c #2, and UE-25c #3, Yucca Mountain, Nye County, Nevada: U.S. Geological Survey Water-Resources Investigations Report 94–4177, 119 p.

Geldon, A.L., Earle, J.D., and Umari, Amjad M.A., 1997, Determination of barometric efficiency and effective porosity, boreholes UE-25 c#1, UE-25 c#2, and UE-25 c#3, Yucca Mountain, Nye County, Nevada: U.S. Geological Survey Water-Resources Investigations Report 97–4098, 17 p.

Geldon, A.L., Umari, Amjad M.A., Earle, J.D., Fahy, M.F., Gemmell, J.M., and Darnell, Jon, 1998, Analysis of a multiple-well interference test in Miocene tuffaceous rocks at the C-hole Complex, May-June 1995, Yucca Mountain, Nevada: U.S. Geological Survey Water-Resources Investigations Report 97–4166, 33 p.

Geldon, A.L., Umari, Amjad M.A., Fahy, M.F., Earle, J.D., Gemmell, J.M., and Darnell, Jon, 2002, Results of hydraulic tests in Miocene tuffaceous rocks at the C-hole Complex, 1995 to 1997, Yucca Mountain, Nye County, Nevada: U.S. Geological Survey Water-Resources Investigations Report 2002–4141, 58 p.

Levenspiel, O., 1972, Chemical reaction engineering, 2d edition: New York, John Wiley and Sons, 578 p.

Luckey, R.R., Tucci, Patrick, Faunt, C.C., Ervin, E.M., Steinkampf, W.C., D'Agnese, F.A., and Patterson, G.L., 1996, Status of understanding of the saturated-zone ground-water flow system at Yucca Mountain, Nevada, as of 1995: U.S. Geological Survey Water-Resources Investigations Report 96–4077, 71 p.

Medina, A., and Carrera, J., 1996, Coupled estimation of flow and solute transport parameters: Water Resources Research, v. 32, no. 10, p. 3063–3076.

Moench, A.F., 1989, Convergent radial dispersion—A Laplace transform solution for aquifer tracer testing: Water Resources Research, v. 25, no. 3, p. 439–447.

Moench, A.F., 1995, Convergent radial dispersion in a double-porosity aquifer with fracture skin—Analytical solution and application to a field experiment in fractured chalk: Water Resources Research, v. 31, no. 8, p. 1823–1835.

Skagius, K., and Neretnieks, I., 1986, Porosities and diffusivities of some nonsorbing species in crystalline rocks: Water Resources Research, v. 22, no. 3, p. 389–398.

Stetzenbach, K.J., and Thompson, G.M., 1983, A new method for simultaneous measurement of Cl^-, Br^-, NO_3^-, SCN^-, and I^- at sub-ppm levels in ground water: Ground Water, v. 21, no. 1, p. 36–41.

Umari, Amjad M.A., 1977, Identification of aquifer dispersivities in two dimensional, transient, groundwater contaminant transport—An optimization approach: Ph. D. dissertation—Cornell University, 122 p.

Umari, Amjad M.A., 1996, An automated curve-matching approach to the analysis of convergent tracer tests—AGU 1996 fall meeting [abs.]: EOS, Transactions, American Geophysical Union, v. 77, no. 46, Suppl., p. F207.

Umari, Amjad, Willis, Robert, and Liu, Philip L-F., 1979, Identification of aquifer dispersivities in two-dimensional, transient groundwater contaminant transport—An optimization approach: Water Resources Research, v. 15, no. 4, p. 815–831.

Wagner, B.J., and Gorelick, S.M., 1986, A statistical methodology for estimating transport parameters—Theory and applications to one-dimensional advective-dispersive systems: Water Resources Research, v. 22, no. 8, p. 1303–1315.

Watermark Computing, 1994, PEST Model-independent parameter estimation—User's manual: Oxley, Australia, Watermark Computing, v5.5 (STN 10289–5.5–00 [161564]), various pagination.

Glossary

Selected terminology used in this report, arranged alphabetically, with Greek symbols at end. Bold terms in the second column are defined in the first column.

TERMINOLOGY	MEANING
actual dimensional time (t)	Time since tracer injection. Same notation, t, as used for **theoretical dimensional time**.
actual field dimensional breakthrough curve	Arithmetic or log-log plot of **actual field dimensional concentration** of tracer measured at the production well plotted against **actual dimensional time** since injection.
actual field dimensional concentration (c)	Actual field concentration of tracer measured in ground water at the production well.
actual field dimensionless breakthrough curve	Arithmetic or log-log plot of **actual field dimensionless concentration** plotted against **actual dimensional time** since injection.
actual field dimensionless concentration (c/c_{max})	**Actual field dimensional concentration** of tracer measured in ground water at the production well normalized by the maximum **actual field dimensional concentration** of tracer for a particular test.
advection traveltime (t_a)	Length of time for a tracer slug to travel from the injection well to the production well by plug flow (pure advection: no dispersion). Equation 1 in text is used to calculate t_a. One of the **input aquifer-property parameters** for the **Moench single- or dual-porosity analytical solution**.
advection-dispersion transport equation	Well-known differential equation for describing ground-water **solute transport,** that is, the movement and spreading of solutes with ground-water flow.
analytical solution method	Analytical, as opposed to numerical, method to solve the **advection-dispersion transport equation**. Specifically, for this report, the **Moench single-porosity analytical solution** (Moench, 1989) and the **Moench dual-porosity analytical solution** (Moench, 1995).
aquifer	Geologic material through which ground-water flow and **solute transport** occur. An aquifer can consist of either: (1) loose material above bedrock and called a porous medium or, (2) fractured bedrock and called an **equivalent porous medium**.
areal flow	Ground-water **flow field** that is contained in the horizontal plane, without a vertical component.
best visual graphical match	A **match** of **BTC**(s) subjectively deemed by the analyst to be the "best" match by overlaying a **type curve** or **theoretical (dimensional or dimensionless) BTC** on the **actual field (dimensional or dimensionless) BTC**. The **input aquifer-property parameters** used for this "best" match are the estimated **parameters**. Compare to **PEST match**.
borehole	A hole drilled into geologic formations.

breakthrough curve (BTC)	Arithmetic or log-log plot of concentration of tracer at the production well plotted against **actual dimensional time** since injection at the injection well. Can be **actual field** (**dimensional or dimensionless**) **BTC** (if actual field measurements) or **theoretical** (**dimensional or dimensionless**) **BTC** (if calculated by either the **Moench single- or dual-porosity analytical solution**). Consists of rising limb and falling limb.
BTC	**Breakthrough curve**.
c	**Actual field dimensional concentration**.
C	**Theoretical dimensional concentration**.
C_D	**Theoretical dimensionless concentration**.
C_i	Reference concentration that relates **theoretical dimensional concentration** and **theoretical dimensionless concentration**. Equation 2 in text is used to calculate C_i.
conservative tracer	Tracer that is nonsorbing; it does not sorb onto rock material that is being tested.
dead-end fractures	**Discontinuous fractures** opening into a portion of the **matrix** where there are no nearby fractures carrying water to be connected to by the **matrix**. This results in stagnant water, a part of the **immobile-water component (storage) of an EPM**.
differential matrix-diffusion delay	Delay of the **actual field dimensionless BTC** and the **theoretical dimensionless BTC** for higher values of **GAMMA** (more diffusion into the **matrix**) relative to the **actual field dimensionless BTC** and **theoretical dimensionless BTC** for lower **GAMMA**.
dimensional time (t)	Either **actual dimensional time** or **theoretical dimensional time**.
dimensionless concentration	Either **actual field dimensionless concentration** or **theoretical dimensionless concentration**.
dimensionless matrix-diffusion coefficient (GAMMA, γ)	Dimensionless **parameter** in **Moench dual-porosity analytical solution** that represents the diffusion of a solute into the **immobile-water component of an EPM**. One of the **input aquifer-property parameters** for the **Moench dual-porosity analytical solution**.
dimensionless storage coefficient (SIGMA, σ)	Dimensionless **parameter** in **Moench dual-porosity analytical solution** that represents the storage of a solute in the **immobile-water component of an EPM**. One of the **input aquifer-property parameters** for the **Moench dual-porosity analytical solution**.

dimensionless time (t_D)	**Actual dimensional time** since tracer injection divided by the **advection traveltime** ($t_D = t \div t_a$). Same notation, t_D, as used for **theoretical dimensionless time.**
discontinuous fractures	Fractures that are not continuous from injection well to pumping well. They can be either part of the **flowing-water component of an EPM** if the discontinuous fractures carry moving water and are connected by **matrix**, which allows flow between the fractures; or they can be part of the **immobile-water component of an EPM** if they open into a portion of the **matrix** where there are no nearby fractures carrying water to be connected to by the **matrix**. This results in **dead-end fractures** and stagnant water.
dual-porosity medium	An **EPM** with a **flowing-water component** and an **immobile-water component**.
dual-porosity partially recirculating solution	Solution developed in this report in which the **Moench dual-porosity analytical solution** (Moench, 1995), derived for a **radially convergent flow field**, is modified to represent **solute transport** in a **partially recirculating flow field**. The modification involves superposition of three **Moench dual-porosity analytical solution**(s) to represent the cumulative effects of three separate **interstreamline pathways** of the tracer between injection well and production well in a **dual-porosity medium**.
EPM	**Equivalent porous medium**.
equivalent porous medium (EPM)	An **aquifer** consisting of fractured bedrock that is assumed to behave like a porous **medium** at some appropriate scale.
flow field	The pattern of ground-water flow as depicted graphically by the pattern of a collection of **streamlines**, either radially convergent, or fully or partially recirculating. In a fully or **partially recirculating flow field**, the **streamlines** first diverge when they emmanate from the injection well, then converge toward the production well. See also **radially convergent flow field**.
flowing-water component of an EPM	Component of an **EPM** that allows ground-water flow in it. Consists, in varying proportions, of (1) interconnected fractures and (2) adjacent **discontinuous fractures** carrying moving water and connected by **matrix**, which allows flow between the fractures. See also **immobile-water component of an EPM**.
flow porosity (ϕ_f)	Porosity of the **flowing-water component of an EPM**. One of the **transport properties** and **input aquifer-property parameters** for the **Moench single- or dual-porosity analytical solution**.
fully recirculating tracer test	See **tracer test**.
GAMMA (γ)	See **dimensionless matrix-diffusion coefficient**.

immobile-water component of an EPM	Component of an **EPM** that does not allow ground-water flow in it, but stores the water (and the solute dissolved in it). A solute gets into this portion of an **EPM** from the **flowing-water component of an EPM** and back out in response to concentration differences between the two components. Consists, in varying proportions, of distant **discontinuous fractures (dead-end fractures)** and the **matrix** between them (portion of **matrix** not contributing to flow).
input aquifer-property parameters	Aquifer-property parameters required as input for the **Moench single- or dual-porosity analytical solution: advection traveltime,** t_a; **dimensionless storage coefficient**, **SIGMA** (σ); **dimensionless matrix-diffusion coefficient**, **GAMMA** (γ); **longitudinal dispersivity**, α_L, in the form of the **Peclet number (PE)**; **transverse dispersivity**; **flow porosity**, ϕ_f; and **matrix (storage) porosity**, ϕ'.
input test-configuration parameters	Tracer test information about the wells, pumping, and tracer required for the **Moench single- or dual-porosity analytical solution**: production rate, distance between injection well and production well, **aquifer** thickness and mixing lengths, and mass of tracer injected and volume of water.
interstreamline pathway	One of the paths taken by water and tracer from the injection well to the production well in a **partially recirculating flow field**. It is defined by two curved bounding **streamlines** (ground-water flow lines) (see fig. 16*A*).
longitudinal dispersivity (α_L)	A **transport parameter** that is a measure of the ability of a porous **medium** to disperse a solute along **streamlines** (ground-water flow lines). One of the **input aquifer-property parameters** for the **Moench single- or dual porosity analytical solutions**.
match	To make a portion of a **Moench type curve** or a **theoretical dimensional or dimensionless BTC** overlie a portion of an **actual field dimensional or dimensionless BTC** to some extent. Various matches are obtained when the analyst varies the **input aquifer-property parameters.** The match can be a **best visual graphical match** or a **PEST match** by the PEST parameter-estimation program. The match can be of the rising limb, of the falling limb, or of the whole **BTC**.
Matching Method 1	In this process, estimates of t_a and **PE** are obtained from closely matching the rising limbs of the **actual field dimensional or dimensionless BTC** with the **type curve** or **theoretical dimensional or dimensionless BTC** using the **Moench single-porosity analytical solution**. The resulting falling limb match may not be very good but good enough to assert that the **medium** is a **single-porosity medium.**
Matching Method 2	In this process, estimates of t_a and **PE** are obtained from loosely matching the whole **actual field dimensional or dimensionless BTC** to the **type curve** or **theoretical dimensional or dimensionless BTC** using the **Moench single-porosity analytical solution**, or the **Modified Moench single-porosity analytical solution**.

Matching Method 3	In this process, estimates of t_a and **PE** are first obtained from closely matching the rising limbs of the **actual field dimensional or dimensionless BTC** with the **type curve** or **theoretical dimensional or dimensionless BTC** using the **Moench dual-porosity analytical solution**. These values then are fixed and **SIGMA** and **GAMMA** are varied and their values estimated from matching the falling limbs, which may not match well. Only a **best visual graphical match** is used for this method.
Matching Method 4	In this process, estimates of t_a and **PE** are first obtained from closely matching the rising limbs of the **actual field dimensional or dimensionless BTC** with the **type curve** or **theoretical dimensional or dimensionless BTC** using the **Moench dual-porosity analytical solution** or the **Modified Moench dual-porosity analytical solution**. With these values of t_a and **PE** used as starting values, the match of the falling limb may be improved by varying **SIGMA** and **GAMMA**, along with t_a and **PE**, and estimating values for all four from matching the whole **BTC**. A **best visual graphical match** or a **PEST match** (nonlinear regression technique) can be used for this method. This method may produce a loose match of the rising limb but may lead to improved matches of the falling limb relative to **Matching Method 3**.
matrix	The part of a fractured tuff rock mass that is not the fractures (fig. 4). For a **single-porosity medium**, the matrix is part of the **flowing-water component of an EPM** because it allows flow through it. For a **dual-porosity medium,** part of the matrix contributes to the **flowing-water component of an EPM,** but part of the matrix does not contribute to flow and is part of the **immobile-water component of an EPM**.
matrix porosity (ϕ')	Porosity of the **immobile-water component of an EPM.** Same as **storage porosity.** One of the **input aquifer-property parameters** for the **Moench dual-porosity analytical solution**.
medium	See **aquifer**.
Moench dual-porosity analytical solution	Solution to the **advection-dispersion transport equation** governing **solute transport** in a **dual-porosity medium** for specific values of **input test-configuration parameters** and **input aquifer-property parameters**, such as **PE**, **GAMMA**, and **SIGMA**, as given in Moench (1995). The solution is represented graphically by a dual-porosity **type curve**, dual-porosity **theoretical dimensional BTC**, or a dual-porosity **theoretical dimensionless BTC**.
Moench input parameters	Parameters required as input for the **Moench single- or dual-porosity analytical solution: input test-configuration parameters** and **input aquifer-property parameters**.

Moench single-porosity analytical solution	Solution to the **advection-dispersion transport equation** governing **solute transport** in a **single-porosity medium** for specific values of **input test-configuration parameters** and **input aquifer-property parameters** as given in Moench (1989). The solution is represented graphically by a single-porosity **type curve**, single-porosity **theoretical dimensional BTC**, or a single-porosity **theoretical dimensionless BTC**.
Moench type curve	Log-log plot of **theoretical dimensionless concentration** at the production well against **theoretical dimensionless time** since injection, obtained from either the **Moench single- or dual-porosity analytical solution**.
normalize	To make the **actual field concentration** dimensionless, by dividing by the maximum **actual field concentration**, which has the same units.
optimal PEST parameters or results	Optimal **PE**, **GAMMA**, and **SIGMA parameter** values resulting from a **PEST match**.
parameter	One of the **input test-configuration parameters** or **input aquifer-property parameters**.
partially recirculating flow field	The pattern of ground-water flow as depicted graphically by the pattern of a collection of **streamlines** resulting from partial **recirculation** in a **tracer test** (reinjecting some of the water pumped from the production well back into the injection well). See also **flow field**.
partially recirculating solution	See **single- or dual-porosity partially recirculating solution**.
partially recirculating tracer test	See **tracer test**.
PE	**Peclet number**.
Peclet number (PE)	**Parameter** equal to r_L, the distance from the production well to the injection well**,** divided by α_L, the **longitudinal dispersivity**, the ability of the **aquifer** to disperse a solute along **streamlines** (ground-water flow lines). One of the **input aquifer-property parameters** for the **Moench single- or dual-porosity analytical solution**.
PEST match	The result from making a portion of a **theoretical** (**dimensional or dimensionless**) **BTC** calculated from the **Moench single- or dual-porosity analytical solution** (Moench, 1989, 1995) executed by the parameter-estimation program, PEST (Watermark Computing, 1994), overlie a portion of an **actual field** (**dimensional or dimensionless**) **BTC** to some extent. The first PEST run starts with the **PE**, **SIGMA**, and **GAMMA** values from a **best visual graphical match**. These initial estimates of **PE, SIGMA,** and **GAMMA** are varied in a series of PEST runs until the sum of squares of differences between actual concentrations on an **actual field** (**dimensional or dimensionless**) **BTC** and theoretical concentrations on a **theoretical** (**dimensional or dimensionless**) **BTC** is minimized. This **PEST theoretical BTC** is the PEST match that determines the associated **PE**, **SIGMA**, and **GAMMA parameter** values that are the **optimal PEST parameters**.

PEST theoretical BTC	**Theoretical** (**dimensional or dimensionless**) **BTC** in a **PEST match** using the **optimal PEST parameters**, as explained under **PEST match**.
porosity	See **flow porosity**, **matrix porosity**, and **storage porosity**.
radially convergent flow field	Ground-water flow pattern resulting from pumping one well in which the **streamlines** converge radially to the well. See also **flow field**.
radially convergent tracer test	See **tracer test**.
recirculation	Process of reinjecting some or all of the water pumped from the production well into the injection well.
robust	**Parameter** estimate not sensitive to the matching method.
SIGMA (σ)	**Dimensionless storage coefficient**.
single-porosity medium	An **EPM** with only a **flowing-water component of an EPM** (no **immobile-water component of an EPM**).
single-porosity partially recirculating solution	Solution developed in this report in which the **Moench single-porosity analytical solution** (Moench, 1989), derived for a **radially convergent flow field**, is modified to represent **solute transport** in a **partially recirculating flow field**. The modification involves superposition of three **Moench single-porosity analytical solution**(s) to represent the cumulative effects of three separate **interstreamline pathways** of the tracer between injection well and production well in a **single-porosity medium**.
solute transport	Movement and spreading of solutes with ground-water flow.
storage	Process of storing immobile water and solute in a portion of an **EPM** (**immobile-water component of an EPM**), as opposed to flow.
storage component of an EPM	Same as **immobile-water component of an EPM**.
storage porosity (ϕ')	Same as **matrix porosity**.
streamline(s)	Curvilinear or straight line along which ground water flows.
swept volume	Volume of water in an **interstreamline pathway**. Because water is continously moving through the **interstreamline pathway**, this volume represents the volume of pore space that water will pass through, or sweep, on its way from the injection well to the production well.
t	**Actual dimensional time** or **theoretical dimensional time**.

t_a	**Advection traveltime**.
t_D	**Dimensionless time** or **theoretical dimensionless time**.
theoretical dimensional BTC	Arithmetic or log-log plot of **theoretical dimensional concentration** at the production well against **theoretical dimensional time** since injection obtained from either the **Moench single- or dual-porosity analytical solution**.
theoretical dimensional concentration (C)	Theoretical breakthrough concentration at the production well (calculated by either the **Moench single- or dual-porosity analytical solution**). $C = C_D \times C_i$
theoretical dimensional time (t)	Obtained from multiplying the **theoretical dimensionless time,** t_D, obtained from either the **Moench single- or dual-porosity analytical solution**, by the **advection traveltime** ($t = t_D \times t_a$). Same notation, t, as used for **actual dimensional time**.
theoretical dimensionless BTC	Arithmetic or log-log plot of **theoretical dimensionless concentration** at the production well against **theoretical dimensional time** since injection obtained from either the **Moench single- or dual-porosity analytical solution**.
theoretical dimensionless concentration (C_D)	Theoretical breakthrough concentration at the production well, equal to the **theoretical dimensional concentration**, C, (calculated by either the **Moench single- or dual-porosity analytical solution**), and normalized by C_i, a reference concentration (defined by equation 2 in the text). $C_D = C/C_i$
theoretical dimensionless time (t_D)	Obtained from either the **Moench single- or dual-porosity analytical solution** and multiplied by the **advection traveltime** to give the **theoretical dimensional time** ($t = t_D \times t_a$).
tracer test	Test conducted in an **aquifer** to estimate its **transport properties**. A tracer solution is injected into an injection well while a production well is pumped. If the water pumped from the production well is not reintroduced into the aquifer, the **flow field** tested is a **radially convergent flow field** and the tracer test is called a radially convergent tracer test. If part of the water pumped from the production well is reintroduced into the aquifer (reinjected into the injection well), the **flow field** tested is a **partially recirculating flow field** and the tracer test is called a partially recirculating tracer test. If all of the water pumped from the production well is reintroduced into the aquifer (reinjected into the injection well), the tracer test is called a fully recirculating tracer test. When the tracer arrives at the production well, an **actual field (dimensional or dimensionless) BTC** is plotted and analyzed for **transport properties** of the **aquifer**.
transport	See **solute transport**.
transport parameter(s)	Same as **transport property**(**ies**).

transport porosity	See **flow porosity**.
transport property(ies)	One of the **aquifer** properties that govern **solute transport** in groundwater flow. Same as transport parameters. See **input aquifer-property parameters** for the **Moench single- or dual-porosity analytical solution**.
transverse dispersivity	One of the **transport properties** representing the ability of the **medium** to disperse a solute in a direction perpendicular to **streamlines**. One of the **input aquifer-property parameters** for the **Moench single- or dual-porosity analytical solution**.
type curve	See **Moench type curve**.
well	**Borehole** with equipment installed that is used to perform a function; for example, injection well or production well.
Greek Symbols	
α_L	**Longitudinal dispersivity**.
γ (GAMMA)	**Dimensionless matrix-diffusion coefficient**.
σ (SIGMA)	**Dimensionless storage coefficient**.
ϕ_f	**Flow porosity**.
ϕ'	**Matrix (storage) porosity**.

ISBN 978-1411320918

Printed on recycled paper